Quantification of Biomechanical Imaging Biomarkers

Sudhakar Tummala

February 9, 2012

Contents

1 Introduction **1**
1.1 Imaging Osteoarthritis and Biomarkers 2
1.1.1 MRI principle 3
1.1.2 Knee Mechanics 5
1.1.3 OA biomarkers and grading 6
1.2 Outline of the Dissertation 7
1.3 Main contributions 8

2 Surface Smoothness: Cartilage Biomarkers for Knee OA beyond the Radiologist **9**
2.1 Introduction 10
2.2 Technical vs. Clinical Validation 11
2.3 Diagnostic Imaging Biomarkers of Osteoarthritis 12
2.4 Cartilage Surface Smoothness Biomarkers and Validation . . 13
2.4.1 Related Work 13
2.5 Population and Image Acquisition 14
2.6 Computational Methods 14
2.6.1 Cartilage Segmentation 14
2.6.2 Curvature Measurement by Curve-evolution framework 15
2.6.3 Statistical Analysis 16
2.7 Regularization effects 16
2.8 Results 17
2.9 Conclusion 18

3 Tibial and Femoral Cartilage Smoothness: Diagnostic markers of early OA? 20
3.1 Purpose . . . 20
3.2 Methods . . . 21
3.3 Results . . . 21
3.4 Conclusion . . . 22

4 Diagnosis of OA by cartilage surface smoothness quantified automatically from knee MRI 23
4.1 Introduction . . . 24
4.2 Materials and Methods . . . 27
4.2.1 Study Population . . . 27
4.2.2 Image acquisition . . . 27
4.2.3 Manual and Automatic Cartilage Segmentation . . . 28
4.2.4 JSW and volume quantification . . . 28
4.2.5 Smoothness Quantification . . . 28
4.2.6 Cartilage Compartments . . . 29
4.2.7 Statistical Analysis . . . 30
4.3 Results . . . 30
4.3.1 Marker precision . . . 31
4.3.2 Smoothness as Diagnostic marker of OA . . . 31
4.3.3 Smoothness as Efficacy Marker . . . 32
4.3.4 Smoothness quantification from manual and automatic segmentations . . . 33
4.4 Discussion . . . 33

5 Automatic Quantification of Tibio-Femoral Contact Area and Congruity 38
5.1 Introduction . . . 39
5.2 Methods . . . 41
5.2.1 Dynamic joint biomechanics . . . 41
5.2.2 Contact Area and Congruity Index formulation . . . 42
5.2.3 Application to medial tibio-femoral joint . . . 44
5.3 Experimental setup . . . 49
5.3.1 Study population . . . 49
5.3.2 Statistical analysis . . . 50

5.3.3 Cross-validation 50
5.4 Results 50
5.4.1 Contact area 51
5.4.2 Congruity index 52
5.4.3 Fixing the parameters 52
5.4.4 Comparison with a related method 53
5.5 Discussion 53
5.5.1 Limitations 56
5.6 Conclusions 58

6 Gender differences in Tibio-Femoral Contact Area and Congruity Index from MRI **59**
6.1 Introduction 60
6.2 Methods 62
6.2.1 Study Population 62
6.2.2 Image Acquisition 62
6.2.3 Cartilage Volume and Joint Space Width Quantification 63
6.2.4 Contact Area and Congruity Index Quantification . . 63
6.2.5 Statistical Analysis 64
6.3 Results 65
6.3.1 Cross-sectional separation of CA at Baseline and at follow-up 65
6.3.2 Cross-sectional separation of CI at Baseline and at follow-up 66
6.3.3 Responsiveness of CA and CI 67
6.3.4 Efficacy of CA and CI 68
6.4 Discussion 68

7 Summary and General Discussion **72**
7.1 Summary 72
7.2 Markers Precision 73
7.3 Diagnosis of OA from CSS, CA and CI 74
7.4 Efficacy of CSS, CA and CI 74
7.5 Prognosis of MTF cartilage loss and JSN 75
7.6 Related Works & Improvements 75
7.7 Limitations 76

7.8 Future Prospects 77

Bibliography **79**

List of Publications **92**

Acknowledgements **94**

List of Figures

1.1 Cartilage contrast with various pulse sequences. (A) Sagittal fat-suppressed T1-weighted 3D GRE image depicting articular cartilage as a high-signal structure in sharp contrast against adjacent low-signal bone, marrow fat, intra-articular adipose, fluid, ligaments and menisci. (B) Sagittal 3D DESS image showing partial-thickness cartilage defect (arrow) over posterior lateral tibial. Note the similarities in contrast properties of fat-suppressed DESS with those of fat-suppressed FSE. (C) Sagittal fat-suppressed IW 2D FSE shows a loose body (arrow) in the patellofemoral compartment. (D) Sagittal T2-weighted 2D FSE image without FS shows a partial-thickness defect (arrow) of the lateral femoral cartilage adjacent to the posterior horn of the meniscus. (E) Sagittal fat-suppressed T2-weighted 2D FSE image of a different knee shows a partial-thickness cartilage defect (arrow) in a similar location (figure and caption reproduced from [79]). 3

1.2 Posterior view of the human knee joint showing the bones and various tissues present in it (figure reproduced from 'Anatomy of Human Body', Henry Grey, fig.348) 4

1.3 Top view of the knee joint showing the medial and lateral meniscus that normally help to speard the contact area and to achieve maximum congruence in the joint (figure reproduced from 'Anatomy of Human Body', Henry Gray, fig.349) 5

1.4 Lateral radiograph showing the bones in the joint, Sagittal slice of an MRI of the knee, MRI enables to visualize other tissues than bone (figures reproduced from 'Atlas of anatomy', Gilroy Anne M et.al. fig. 25.3.B and fig.25.18.) 6

2.1 Simplified illustration of typical stages of OA where the cartilage integrity is initially lost (yellow icons are chondrocytes) eventually leading to denudation. The underlying bone experiences increased turnover (red icons are osteoblasts) and deformations leading to subchondral thickening and osteophytes. Loss of surface integrity occurs during early radiographic OA and may be measured as surface smoothness from MRI (figure adapted from [82]). 12
2.2 Medial Tibio-Femoral cartilage compartment and it's sub-compartments 16
2.3 Variation of RMS CV (left) and ESS (right) for Manual and Automatic Segmentations from iteration 0 to 30 in case of Tibial. 17

4.1 In early osteoarthritis, loss of the interior cartilage structure and loss of surface integrity occur before cartilage loss, sclerosis of underlying bone, and joint space narrowing. . . 26
4.2 The smoothness markers at each level of OA for the tibial (3A) and femoral (3B) compartments. The mean smoothness score is given with standard error of the mean given as error bars. The KL $\leq$ 1 and KL > 1 sub-populations are compared to the left of the dashed lines. To the right, the scores are given for each level of KL. Statistically significant differences are shown as * for $p < 0.05$, ** for $p < 0.01$, *** for $p < 0.001$, **** for $p < 0.0001$. 35

5.1 Showing two artificial surfaces in contact and illustration of how the normal vector and the principal curvatures are located in the contact region of S_a. The X, Y and Z axes form the global coordinate system. The tangent plane is perpendicular to the normal vector $\overline{n_a}$. The red zone S_a^c is the region where S_a and S_b are in contact. The $\overline{p_a^1}$ and $\overline{p_a^2}$ are the maximal and minimal principal directions respectively and $\overline{v}$ is the direction along which we computed the normal curvature. Angle α is the angle between $\overline{p_a^1}$ and $\overline{v}$. 43
5.2 The Bland-Altman plots of CA and CI showing the agreement between scan-rescan values. SD: standard deviation. . 50
5.3 Congruity map shown over the CA for a healthy knee used in the cross-validation. Red indicates higher congruity, generally observed in the central regions. Blue indicates lower congruity, generally observed all over the CA and mostly around the periphery. It is plotted at a curvature scale of 2.4 mm and 4 curvature flow iterations. 51
5.4 The scatter plot between our CI and the CI in [4]/[47] based on the baseline knees including all KL. The red line is the best fit. 53
5.5 Cross-sectional separation of healthy and different KL using the CA and the CI at baseline for the fixed parameters (2.4 mm curvature scale, 4 curvature flow iterations). *P < 0.05, **P < 0.01, ***P < 0.001, ****P < 0.0001. 55

6.1 Cross-sectional separation of healthy and different KL for male and female subjects based on Contact Area and Congruity Index at baseline. Contact Areas were higher for female after adjusted for tibial bone width. Congruity indices were smaller for female knees. The stars indicate the statistical significance computed from Students t-test. *P < 0.05, **P < 0.01, ***P < 0.001, ****P < 0.0001. 68

List of Tables

1.1 The table contains the definition of KL used for grading the severity of OA from radiographs. KL 0 is healthy; KL 1 early OA and KL 2 is definite OA, KL 3 and above is graded as advanced OA [60]. 7

2.1 Diagnostic scores from smoothness measurements based on manual and automatic segmentations at 20 iterations. Com: Compartment, T: Tibial, F: Femoral, FA: Femoral Anterior, FC: Femoral Central, FP: Femoral Posterior. 18

3.1 Diagnostic scores from smoothness measurements to separate A: KL 0 & KL > 0, B: KL ≤ 1 & KL > 1. Com: Compartment, T: Tibial, F: Femoral, FA: Femoral Anterior, FC: Femoral Central, FP: Femoral Posterior. *p < 0.05, **p < 0.01, ***p < 0.001, ****p < 0.0001. 22

4.1 Description of the study population with scan count, listing minimum-maximum (mean) values of age, Body Mass Index (BMI), gender and the distribution across the degrees of OA given by the KL Index (0 to 4). 31

4.2 The RMS CV, mean and standard deviation (SD) values for the markers joint space width JSW, volume, and smoothness in each medial compartment are given. The compartments are given as tibio-femoral (TF), tibial (T), femoral (F), femoral anterior (FA), femoral central (FC), and femoral posterior (FP). 31

4.3 Diagnostic scores for joint space width (JSW), cartilage volume, and smoothness quantified in the medial compartment for separating KL ≤ 1 and KL > 1 sub-populations. The compartments are given as tibio-femoral (TF), tibial (T), femoral (F), femoral anterior (FA), femoral central (FC), and femoral posterior (FP). Statistically significant differences are shown as * for p < 0.05, ** for p < 0.01, *** for p < 0.001, **** for p < 0.0001. 32
4.4 The linear correlations between change in cartilage surface smoothness and JSN and cartilage volume loss for each compartment. The compartments are given as tibio-femoral (TF), tibial (T), femoral (F), femoral anterior (FA), femoral central (FC), and femoral posterior (FP). Statistically significant differences are shown as * for p < 0.05, ** for p < 0.01, *** for p < 0.001, **** for p < 0.0001. 33
4.5 Diagnostic scores for cartilage smoothness quantifications in the medial compartments based on manual and automatic segmentations for a subset of 114 scans. The compartments are given as tibio-femoral (TF), tibial (T), femoral (F), femoral anterior (FA), femoral central (FC), and femoral posterior (FP). Statistically significant differences are shown as * for p < 0.05, ** for p < 0.01, *** for p < 0.001, **** for p < 0.0001. 34

5.1 Contact area and Congruity Indices mean and SD values for KL 0, KL 1, KL 2, KL 3 subjects respectively for scan and rescanned knees. Fixed parameters were used (2.4mm curvature scale and 4 curvature flow iterations). N: number of knees 48
5.2 Contact Area and Congruity Indices mean and SD values for KL 0, KL 1, KL 2, KL 3/4 subjects respectively at baseline. Fixed parameters were used (2.4mm curvature scale and 4 curvature flow iterations). N: number of knees 52
5.3 The longitudinal SRM of CA and CI for KL 0, KL 1, KL 2, and KL 3/4 knees respectively. Fixed parameters were used (2.4 mm curvature scale and 4 curvature flow iterations). N: number of knees 52

5.4 Comparison of our proposed method with the method in [4]/[47] for cross-sectional separation tasks using CI at baseline. Fixed parameters were used (2.4mm curvature scale and 4 curvature flow iterations). The Significance of Difference between the AUC values in the 2nd and 3rd columns is also measured using [22], denoted as P_S. *P < 0.05, **P < 0.01, ***P < 0.001, ****P < 0.0001. . 54

5.5 Statistical scores to show the ability of the CA (top rows) and the CI (bottom rows) to separate different groups cross-sectionally at baseline. *p < 0.05, **p < 0.01, ***p < 0.001, ****p < 0.0001. SD: standard deviation. 54

6.1 Table showing the number of knees (N), Age (in years) and BMI (kg/m^2) for male and female subjects used in the evaluation at Baseline (288) and at follow-up (245) with respect to KL index. Stars indicate the significance of difference between the genders for Age and BMI for that specific KL index. The significance of difference between genders was added to the female demographic. *p < 0.05, **p < 0.01, ***p < 0.001, ****p < 0.0001. 65

6.2 The table shows CA and CI values of Male and Female at Baseline as well as at Follow-up. The significance of difference between genders computed as p-value from t-test was added to the female values. M: Male, F: Female, CA: Contact Area, CI: Congruity Index. *p < 0.05, **p < 0.01, ***p < 0.001, ****p < 0.0001. 66

6.3 The sensitivity to change over 21 months for CA and CI for Male and Female subjects for Healthy (KL 0), early OA (KL 1), and OA (KL > 1) were listed. SRM: Standardized response mean, CA: Contact Area, CI: Congruity Index. 68

6.4 Correlations of CA and CI longitudinal percentage changes with tibio-femoral cartilage volume percentage change, JSW percentage change for male and female subjects listed for Healthy (KL 0), early OA (KL 1) and OA (KL > 1) subjects. CA: Contact Area. CI: Congruity Index. M: Male, F: Female, MTF: medial tibio-femoral, JSW: joint space width. *p < 0.05, **p < 0.01, ***p < 0.001, ****p < 0.0001. 70

Abstract

Osteoarthritis (OA) is a debilitating musculoskeletal disorder in the elderly and also a major burden for healthcare economy in western countries. Biomechanics may play a vital role in the early stages of OA. The dissertation presents refinements of exiting method for quantification of Cartilage Surface Smoothness (CSS), and novel methods to quantify Contact Area (CA) and Congruity Index (CI) in the Medial Tibio-Femoral (MTF) cartilage compartment non-invasively using low-field magnetic resonance imaging (MRI).

Initially, to reduce the voxellation effects, the MTF binary cartilage compartments were regularized using mean curvature flow in a level-set formulation before quantifying CSS, CA and CI. The first and second order Gaussian derivatives of the signed distance representation of level-set surfaces were computed and used for the computation of the CSS as inverse of local mean curvature.

The CA was quantified by employing the voxel width as threshold. The local CI was quantified in the CA by assessing first and second order general surface features and associating them. The quantifications were validated on a longitudinal study population from the greater Copenhagen area. The CA was significantly different between healthy and early OA subjects. The CI was also able to separate healthy from early OA.

The CSS and CI performed better than MTF volume for diagnosis of early radiographic OA. Further, the CSS, CA and CI showed suitable as efficacy markers by demonstrating strong correlations with percentage longitudinal changes with MTF cartilage volume. Therefore, the CSS, CA and CI

may be the denominators in the OA progression.
The automatic segmentations also in general allowed the CSS/CS/CI performed equally or better than those from manual segmentations for diagnosis. Female MTF joints demonstrated greater normalized CAs and lower CIs. The lower CIs may help to explain the more prevalence of female OA. Future work could focus on validation of these markers on larger study populations.

Key Words: knee OA, smoothness, contact area, congruity index, machine learning

Chapter 1

Introduction

Musculoskeletal disorders are debilitating factors especially in the elderly. These factors are responsible for 3.4 percentage of gross domestic product for their burden in some western countries [12, 23, 28]. One of the musculoskeletal disorders, Osteoarthritis (OA) is a major health concern worldwide that frequently affects the major load-bearing joints in the body. OA is a whole joint disease characterized as clinical and structural deterioration. It affects the individual's quality of life, by reducing the joint mobility and inducing pain [84]. There have been several demonstrated risk factors responsible for the disposition and progression of OA [38]. The systemic or non-modifiable risk factors are the age, and the gender whereas the non-systemic and modifiable risk factors are the BMI, injury/trauma, etc. OA is a complex disease where the etiology is the combination of biomechanical, biochemical and other factors [38]. Therefore, biomechanical factors may very likely play a significant role in the predisposition of

OA. Currently, there is no cure for OA and controlling symptoms is the only treatment strategy. Symptoms control needs a surgery in most of the cases. Hence, there is a necessity to detect the disease at the early stages and reverse/halt it before it becomes irreversible to prevent the high costs incurred for joint replacement surgery (JRS). The JRS is not a cost effective choice for the developing countries.

The novel biomarkers may help to better understand the etiology, facilitate early diagnosis, or enable prediction of disease progression, or to test the efficacy of a drug in a clinical trial [6]. Since the advanced stages of OA are quite likely irreversible [82], new treatments focussed at the earlier stages may have a higher chance of preventing progression or even curing the disease [7].

1.1 Imaging Osteoarthritis and Biomarkers

Imaging is a technique to visualize inside the body non-invasively and it plays a major role in today's healthcare research. Imaging helps to monitor the efficacy of a drug in the disease modification in a non-invasive manner. The traditional candidate currently for OA (US Food and Drug Administration (FDA) approved) is the joint space narrowing (JSN) measured from radiographs. The radiograph has the advantages of low cost and lower acquisition time. However, MRI provides three dimensional structure where as a radiograph provide only the two dimensional structure. Another demerit of radiographs is also that it may take several years to show any significant decrease in joint space width (JSW), which increases the economic burden of a clinical trial. Also, the correlation of JSN with pain is not well documented/understood. The use of magnetic resonance imaging (MRI) could allow studying other tissues that may indicate the disease progression faster than JSW. The MRI enables to look at the joint as a whole organ and score the disease severity using all visible tissues such as whole-organ magnetic resonance imaging score done in [78]. The prominent marker from MRI currently employed in clinical trials is the cartilage volume. Cartilage quality and local biomechanical factors may play a role at the early stages of the disease. In the knee, some of the markers that are associated to cartilage quality/early surface asperities and

to biomechanics are the Cartilage Surface Smoothness (CSS), Contact Area (CA) and Congruity Index (CI).

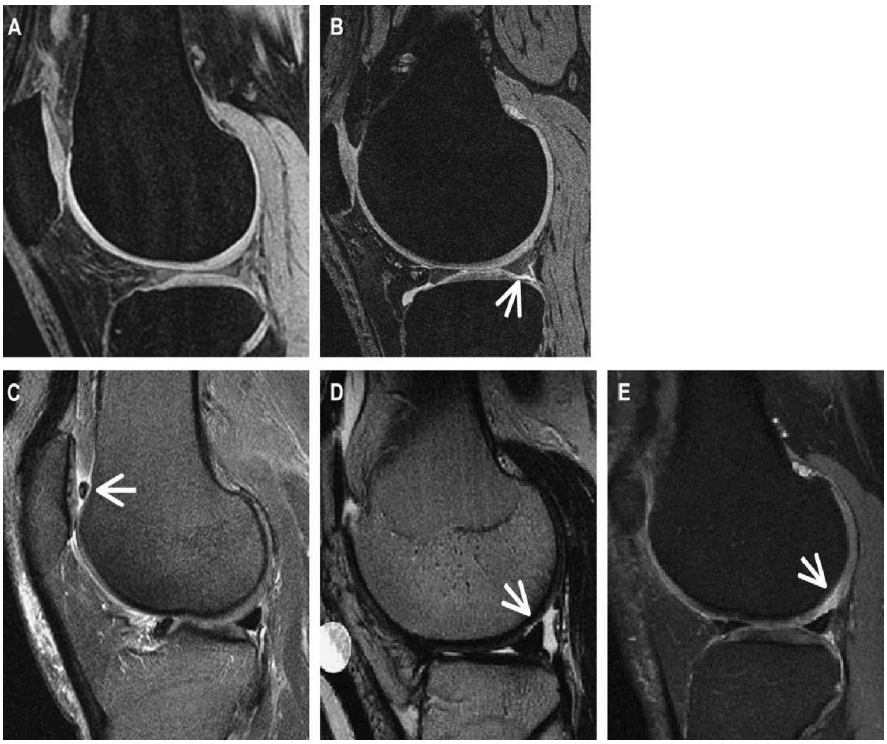

Figure 1.1: Cartilage contrast with various pulse sequences. (A) Sagittal fat-suppressed T1-weighted 3D GRE image depicting articular cartilage as a high-signal structure in sharp contrast against adjacent low-signal bone, marrow fat, intra-articular adipose, fluid, ligaments and menisci. (B) Sagittal 3D DESS image showing partial-thickness cartilage defect (arrow) over posterior lateral tibial. Note the similarities in contrast properties of fat-suppressed DESS with those of fat-suppressed FSE. (C) Sagittal fat-suppressed IW 2D FSE shows a loose body (arrow) in the patellofemoral compartment. (D) Sagittal T2-weighted 2D FSE image without FS shows a partial-thickness defect (arrow) of the lateral femoral cartilage adjacent to the posterior horn of the meniscus. (E) Sagittal fat-suppressed T2-weighted 2D FSE image of a different knee shows a partial-thickness cartilage defect (arrow) in a similar location (figure and caption reproduced from [79]).

1.1.1 MRI principle

When the body is placed inside a strong magnetic field of the scanner, the magnetic moments of hydrogen molecules become aligned with the

direction of the field. Then an external radio frequency (RF) field is turned on so that the photons of this RF field have just the right energy, known as the resonance frequency, to be absorbed and flip the spin of the aligned hydrogen protons in the body part of interest. The frequency at which the protons resonate depends on the strength of the applied magnetic field. After the RF field is turned off, those protons which absorbed energy revert to the original lower-energy spin-down state. During this process, they release the difference in energy as a photon, and the released photons are detected by the scanner as an electromagnetic signal which is reconstructed as an image using Fourier Transform techniques [44]. The traditional images are produced under scanner parameters T1, T2, proton density with different pulse sequences such as gradient echo and spin echo etc. Various MRI protocols that could be used in OA research depending on the application were compared and detailed in [79].

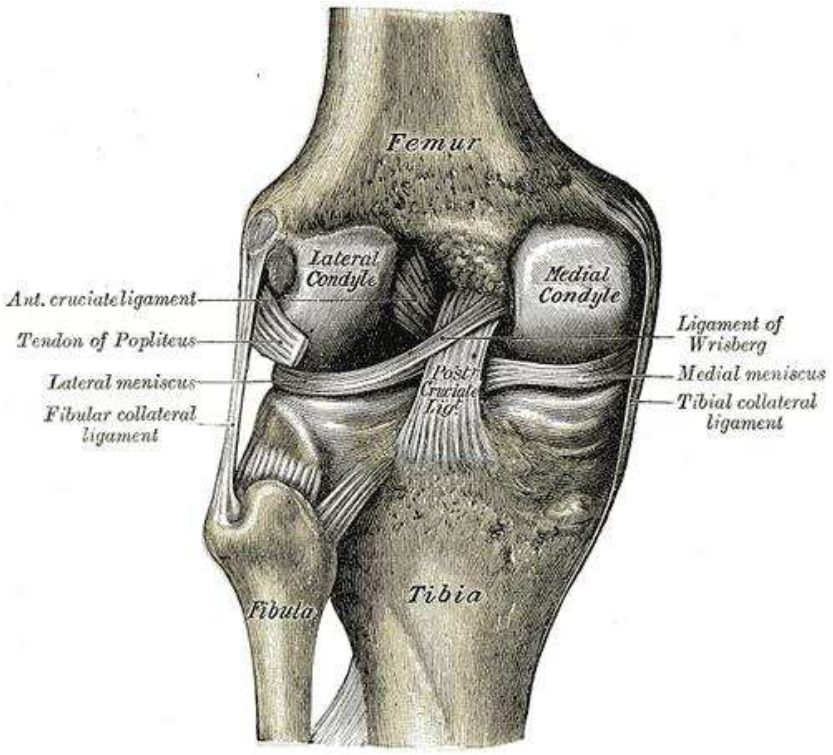

Figure 1.2: Posterior view of the human knee joint showing the bones and various tissues present in it (figure reproduced from 'Anatomy of Human Body', Henry Grey, fig.348)

.

1.1.2 Knee Mechanics

The knee is one of the major synovial joints in the body. Figure 1.1 shows a human knee joint with the bones that constitute the joint and the cartilage tissues. The cartilage, a smooth slippery tissue that covers the end of tibia and femur transfers the load effectively across the joint during various daily activities. The synovial fluid facilitates almost frictionless motion by providing lubrication. The C-shaped tissues called the menisci (figure 1.2) acts as shock absorbers and usually carries significant amount of the load exerted in the joint and also facilitates in joint stability [99]. Also, the menisci help to achieve maximum contact area which further increases the congruence of the joint. The ligaments and tendons provide the static and dynamic stability by mediating the motion of the knee during various daily activities. The knee has six degrees of freedom that include flexion/extension, abduction/adduction, internal/external rotation. The major motion is the flexion/extension whereas the other two pair of motions occur during the major motion.

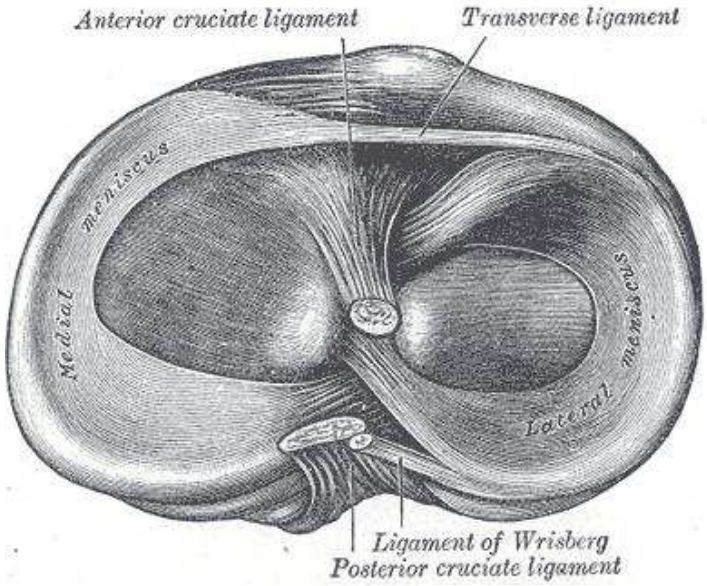

Figure 1.3: Top view of the knee joint showing the medial and lateral meniscus that normally help to speard the contact area and to achieve maximum congruence in the joint (figure reproduced from 'Anatomy of Human Body', Henry Gray, fig.349)

.

1.1.3 OA biomarkers and grading

Biomarker is a characteristic that is objectively measured and evaluated as an indicator of normal biological processes, pathogenic processes or pharmacologic responses to a therapeutic intervention [27]. Since OA is a complex disease involving several factors, novel biomarkers targeting the early stages of the disease are needed to understand the disease onset. The current imaging biomarkers include Kellgren & Lawrence Index (KL), JSW from radiographs; cartilage volume/thickness, cartilage surface area, cartilage homogeneity, cartilage surface curvature, bone structure etc. from MRI [25, 26, 76].

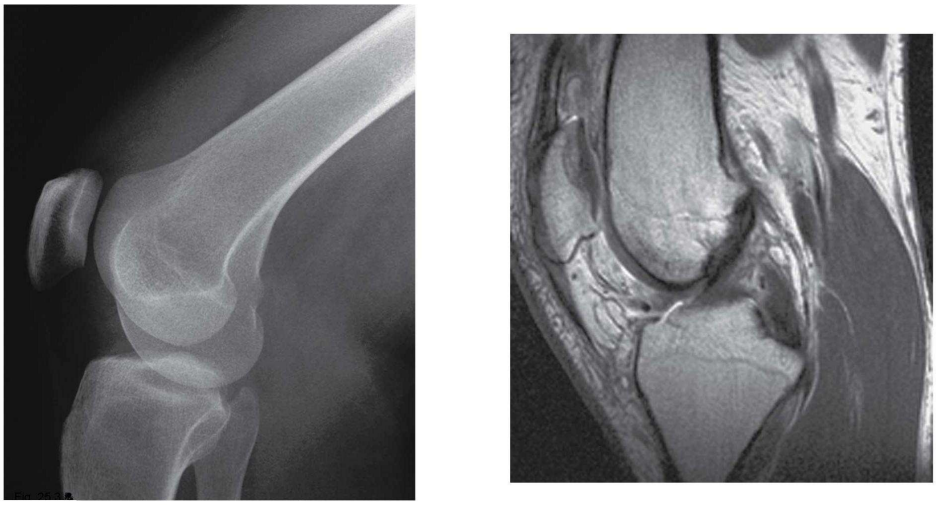

Figure 1.4: Lateral radiograph showing the bones in the joint, Sagittal slice of an MRI of the knee, MRI enables to visualize other tissues than bone (figures reproduced from 'Atlas of anatomy', Gilroy Anne M et.al. fig. 25.3.B and fig.25.18.)

.

The gold standard diagnostic marker for OA currently is KL from the radiograph. The grading system used to assess the severity of OA from radiographs is listed in Table 1.1. The disadvantage of radiographs is that they does not allow direct visualization of cartilage, the amount of cartilage in the joint is manifested as joint space width (JSW) (see figure 1.3a to visualize a radiograph used for the measurement of JSW). Since MRI enables to visualize all the tissues in the joint (figure 1.3b), it is pertaining to develop a gold standard marker from it for early diagnosis before the

disease state becomes irreversible as proposed in [50,51]. Moreover, the KL index was weakly correlated to the pain and physical symptoms [11, 63]. Since OA is a disease of the whole joint it is of interest to examine all the tissues that might be affected or involved during the initiation and progression of OA. Therefore, the focus of the dissertation is on the quality of the articular cartilage and on biomechanics.

Table 1.1: The table contains the definition of KL used for grading the severity of OA from radiographs. KL 0 is healthy; KL 1 early OA and KL 2 is definite OA, KL 3 and above is graded as advanced OA [60].

KL 0	Normal
KL 1	Doubtful narrowing of joint space and possible osteophyte lipping
KL 2	Definite osteophyte and possible narrowing of joint space
KL 3	Moderate multiple osteophytes, definite narrowing of joint space, some sclerosis, and possible deformity of bone contour
KL 4	Large osteophytes, marked narrowing of joint space, severe sclerosis, and definite deformity of bone contour

A biomarker is to be able to diagnose the disease early so that the need for joint replacement surgery could be delayed or abandoned. It is of high interest that any marker demonstrates a significant correlation with pain/function and physical symptoms. The novel markers may also help to reduce the length of a clinical trial for the invention of disease modifying osteoarthritis drugs.

1.2 Outline of the Dissertation

Early detection of the disease is important so that we could treat it better. Biomechanics could be one of the factors that alter during early stages of OA. Biomarkers that could be developed from the biomechanics are CSS, CA, CI, friction,etc. Therefore, the main content of the dissertation is focussed on quantification of biomarkers and their validation that is presented in several chapters. The 2^{nd} Chapter presents the refinement of CSS quantification framework and validates it's ability on the tibial

and femoral sub-compartments (two sources of segmentations were used). The 3^{rd} Chapter demonstrates the cross-sectional separation of healthy and early OA, healthy and OA from CSS. The 4^{th} Chapter exemplifies the diagnosis and monitoring progression of OA from the CSS. The 5^{th} Chapter presents automatic quantification of the CA and the local CI in the MTF joint. The 6^{th} Chapter presents the gender differences in the CA and the local CI using the methods described in 5^{th} Chapter. The last Chapter, Chapter 7, presents the summary and general discussion of the dissertation content.

1.3 Main Contributions

The main contributions of the thesis are:
• Contrasting the precision and ability to separate healthy and OA for CSS based on manual and automatic segmentations (Chapter 2).
• Ability of CSS of tibial, femoral and femoral sub-compartments for diagnosis of KL 0 & KL > 0 and KL ≤ 1 & KL > 1 is compared (Chapter 3).
• Validation of the CSS (early surface asperities) quantification framework for diagnosis and monitoring of OA from the medial tibial and femoral compartments and its sub-compartments (Chapter 4).
• Quantification of cartilage-cartilage CA to indirectly assess the meniscal extrusion or subluxation during early OA (Chapter 5).
• A novel quantification framework for quantification of local CI is proposed. The CI is related to local conformity of the surfaces which needs to be good for optimum transfer of loads across the compartments (Chapter 5).
• The CI was quantified in the contact area by assessing the first (normal vectors) and second (normal curvatures) order general surface features. The 1^{st} and 2^{nd} order Gaussian derivatives were computed from the signed distance function of the level set representation of the binary segmentations (Chapter 5).
• Gender differences in the MTF joint CA and CI stratified according to KL index are investigated and discussed (Chapter 6).

Chapters 2-6 are the 'raw' papers/manuscripts with only the references excluded.

Chapter 2

Smoothness quantification framework is matured to handle multi-compartments. Main results are shown in Table 2.1.

Surface Smoothness: Cartilage Biomarkers for Knee OA beyond the Radiologist

Tummala S, Dam EB
This chapter is based on the publication in SPIE Medical Imaging 2010, San Diego, USA

Fully automatic imaging biomarkers may allow quantification of pathophysiological processes that a radiologist would not be able to assess reliably. This can introduce new insight but is problematic to validate due to lack of meaningful ground truth expert measurements. Rather than quantification accuracy, such novel markers must therefore be validated against

clinically meaningful end-goals such as the ability to allow correct diagnosis. We present a method for automatic cartilage surface smoothness quantification in the knee joint. The quantification is based on a curvature flow method used on tibial and femoral cartilage compartments resulting from an automatic segmentation scheme. These smoothness estimates are validated for their ability to diagnose osteoarthritis and compared to smoothness estimates based on manual expert segmentations and to conventional cartilage volume quantification. We demonstrate that the fully automatic markers eliminate the time required for radiologist annotations, and in addition provide a diagnostic marker superior to the evaluated semi-manual markers.

2.1 Introduction

Imaging biomarkers have traditionally been focused on helping the radiologist in performing measurements that are otherwise time-consuming or possibly prone to inter-observer variation. Examples of this are volume computation of anatomical structures like the heart chambers or of pathological structures such as tumors. For two-dimensional (2D) scans (e.g. radiographs) manual segmentation can provide the volume with relatively little effort. For data of higher dimensionality (e.g. three-dimensional (3D) brain MRI or gated heart CT sequences (3+1D)), manual segmentation or annotation in general may be so time-consuming or challenging that it is unfeasible for clinical applications [59, 62, 98]. Then imaging methods can help lessen the radiologist burden. This is also the case when the inter-observer variation is so large that multiple radiologist readings are required to obtain sufficient precision, e.g. mammography readings in breast cancer screening programs. Imaging biomarkers can now replace the second radiologist [4]. In all these cases, imaging methods may help solve existing problems with known biomarker solutions. From a clinical point of view, the contribution is essentially to improve the existing work flow - or possibly even make an otherwise too resource consuming marker clinically feasible.
However, imaging biomarkers can also provide measurements beyond automation of known radiologist readings. A first step is to provide quan-

titative markers to replace qualitative scores. One example is to replace the semi-quantitative 24-step aorta calcification scoring method [58] with a continuous quantitative biomarker. This change can be crucial for measuring small changes in longitudinal clinical studies.
Common for the imaging biomarkers mentioned above is that validation seems straight-forward. Repeated, manual readings from trained radiologist can be used for accuracy (or correctness) and precision (or reproducibility) validation. Accuracy is important for diagnostic or prognostic markers whereas precision is also important for efficacy markers (following BIPED terminology [6]. Availability of golden standard measurements does not necessarily make validation trivial, but there exists methods for performing validation even accounting for variation in the expert annotations (e.g. STABLE [100]). However, when the imaging biomarkers go beyond traditional radiology, validation becomes challenging due to lack of golden standard data.

2.2 Technical vs. Clinical Validation

Imaging biomarkers beyond existing radiological scores are surfacing. Particularly, for 3D or 3+1D data the human perception is limited since the scans are observed through partial data such as orthogonal slices or volume rendering. This challenges the radiologist in forming a mental picture of the anatomy or of structural/textural properties in 3D. For instance, it is challenging for the radiologist to provide a manual scoring for the connectedness between brain regions that can be computed by tractography performed on diffusion-tensor MRI [101]. For a fiducial connectedness biomarker, it is very challenging to perform a validation of the measurement accuracy. Instead, even recent papers on tractography use illustrative examples and proof-of-concept validations (e.g. [33]). Even if precision validation could be possible using repeated scans, a non-invasive accuracy evaluation would be challenging.
This illustrates the challenge in validating novel imaging biomarkers - which creates a limiting factor in clinical acceptance. However, for the class of imaging biomarkers designing to be used in clinical studies, it is possible to perform a proper quantitative validation, even with no golden

standard quantification data. The validation can be performed by validating the decision that the marker supports rather than the marker's technical performance. For instance, a prognostic marker inspecting textural mammography patterns beyond density can be validated for the ability to predict breast cancer using historical data [83].
In short, even when technical validation is not feasible, clinical validation based on hard clinical end-points can be straightforward. If the aim is clinical acceptance or FDA approval, clinical validation is anyway the deciding benchmark. The validation measurements should then naturally be those used by clinical papers (for clinical validation scores for different biomarker categories, see [6, 61]).

2.3 Diagnostic Imaging Biomarkers of Osteoarthritis

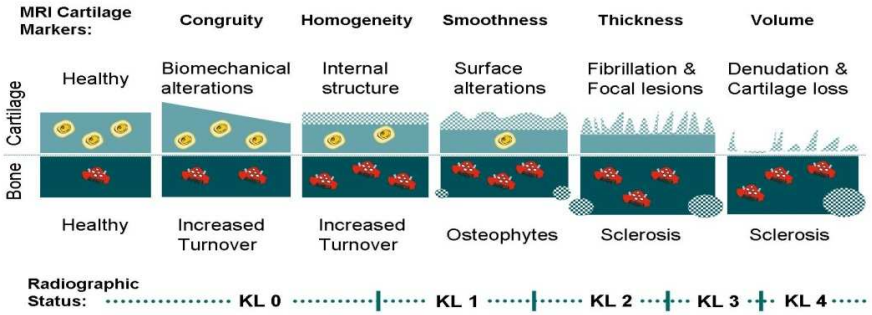

Figure 2.1: Simplified illustration of typical stages of OA where the cartilage integrity is initially lost (yellow icons are chondrocytes) eventually leading to denudation. The underlying bone experiences increased turnover (red icons are osteoblasts) and deformations leading to subchondral thickening and osteophytes. Loss of surface integrity occurs during early radiographic OA and may be measured as surface smoothness from MRI (figure adapted from [82]).

A natural candidate as both diagnostic and efficacy imaging biomarker of OA is cartilage volume measured from MRI. However, since cartilage loss is preceded by a loss of structural integrity (as illustrated in Figure 2.1), markers of cartilage quality would possibly allow earlier diagnosis than a cartilage volume marker. However, whereas cartilage volume is quan-

tifiable by manual segmentation by an expert radiologist, effects linked to the earlier stages of OA are not easily quantifiable by a radiologist in a continuous marker.

2.4 Cartilage Surface Smoothness Biomarkers and Validation

In this paper, we present methods for fully automatic quantification of the cartilage surface smoothness for the tibio-femoral joint. Specifically, we quantify the smoothness for the medial tibial and femoral compartments and for three femoral sub-compartments: anterior, central, and posterior. Golden standard measurement of cartilage smoothness could be quantified by means of arthroscopy. However, due to the invasiveness (and the inherent risk of synovial infection) this is not feasible for clinical studies and not attractive for early diagnosis prior to clinical symptoms in general. We validate the smoothness markers by the applicability for a clinical study - most importantly defined by the estimated sample size (the number of subjects required for the study). The validation is carried out both for smoothness measurements performed from manual segmentations as well as from automatic segmentations.

2.4.1 Related Work

Both Hohe et al ([49]) and Terukina et al ([96]) have previously analyzed cartilage surface curvature from MRI. In both cases, the curvature analysis was performed at large scale meaning that the measurements related to joint congruity rather than smoothness. Surface roughness has been measured acoustically by ultrasound in a feasibility study [20]. However, due to the invasiveness, this method is not feasible for clinical practice.
Earlier versions of the smoothness quantification method used here have been published [39, 40]. The previous version analyzes the tibial cartilage only and was evaluated for accuracy against artificial data [39] and for precision and the diagnostic ability (by p-value) [40].

2.5 Population and Image Acquisition

This study includes 114+31+25 scans. The evaluation was done on 114 scans with the test subjects having age 21-78 (mean 55), BMI 20-38 (mean 27), 54% female and varying degrees of radiographic OA from KL 0 to 4 (51, 28, 15, 20, 0). For the precision evaluation 31 knees were rescanned a week after from the above 114 knees. Additional 25 knees not included in 114, were used for training of the automatic segmentation method. A similar distribution of demographics was present in rescanned and training set as in the case of evaluation set. Radiographs were acquired in the load-bearing semi-flexed position using the SynaFlex (Synarc) and the KL index was determined in the medial tibio-femoral joint. We investigated in the medial tibio-femoral joint since OA is most common there [34]. MRI scans with near-isotropic voxels were acquired from a Turbo 3D T1 sequence from a 0.18T Esaote scanner (40^0 flip angle, repetition time 50 milliseconds, echo time 16 milliseconds, scan time 10 minutes), with approximate spatial-resolution of 0.7 mm x 0.7 mm x 0.8 mm. Slices were acquired in non-load bearing supine position. For more detail on the population and the scans, see [25].

2.6 Computational Methods

2.6.1 Cartilage Segmentation

For all MRI scans, the medial tibial and femoral cartilage compartments were segmented manually by slice-wise delineation by a radiologist and by a fully automatic segmentation algorithm. The automatic method was a voxel classification algorithm based on a k-nearest-neighbor (kNN) classifier trained on the 25 training scans using a feature bank of Gaussian derivatives, intensity, position, and gauge invariant geometric features [41].

2.6.2 Curvature Measurement by Curve-evolution framework

We measure cartilage smoothness as the (inverse) surface curvature. Intuitively, the curvature of a surface is the degree by which it deviates from being flat. However, since the segmentations are represented as binary volumes, regularization is needed in order to avoid voxellation effects. We regularize by a mean curvature flow on the segmented cartilages evolving the surfaces using a level set implementation. To ensure curve evolution robustness, the segmentations are super-sampled (each voxel become 5x5x5) followed by isotropic Gaussian blurring at scale 1 mm. In the level set formulation, the mean curvature flow is described by

$$\frac{\partial \phi}{\partial t} = k_M |\nabla \phi| = [\nabla(\frac{\nabla \phi}{|\nabla \phi|})]|\nabla \phi| \tag{2.1}$$

Where $|\nabla \phi|$ is the gradient of the level set representation ϕ and k_M is the mean curvature. The flow is implemented by a standard; iterative forward/Euler scheme using a step-size of 0.15 ensures the numerical behavior. Smoothness is then measured using the k_M map on the surface facing the synovium i.e. the superior and inferior surfaces for the tibial and femoral compartments, respectively.
The cartilage surface with high curvature values will move towards lower curvatures as the flow progresses. The key parameter in the algorithm is the number of iterations in the curvature flow. The impact of this parameter is analyzed below.

The femoral compartment was further divided into anterior, central, and posterior sub-compartments based on the anterior-posterior width of the femoral compartment (shown in Figure 2.2). The first quarter is named as femoral posterior sub-compartment, central femoral sub-compartment is taken from first quarter to third quarter, and the last quarter is named as femoral anterior sub-compartment. The splitting of femoral cartilage into sub-compartments was validated by visual inspection on several scans, includes healthy and diseased.

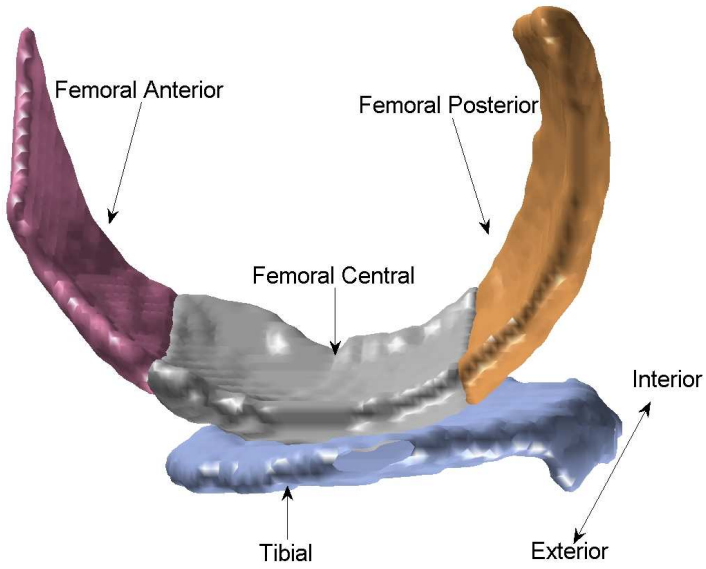

Figure 2.2: Medial Tibio-Femoral cartilage compartment and it's sub-compartments

2.6.3 Statistical Analysis

The precision is quantified as scan-rescan root mean squared coefficient of variation (RMS CV). As shown in Figure 2.1 the cartilage may lose smoothness at around the stage of KL1. So, we evaluated the diagnostic abilities for splitting KL ≤ 1 vs. KL > 1 by the p-value from an unpaired Student's t-test (p) and the corresponding estimated required sample size (ESS) estimated by power analysis [61] with significance level 0.05 and power 0.8. The odd's ratio for ROA was computed using the marker median as threshold (OR). Finally, accuracy for each marker was evaluated by the area under the ROC curve (AUC).

2.7 Regularization effects

The key parameters in the algorithm are the super-sampling factor prior to curvature flow and the number of iterations in the curvature flow. The optimization graphs were obtained for super-sampling factor and number of iterations for tibial, femoral cartilage smoothness. Figure 2.3 shows

precision (RMS CV) and sample size (ESS) at different iterations for the smoothness marker used on manual/automatic segmentations.

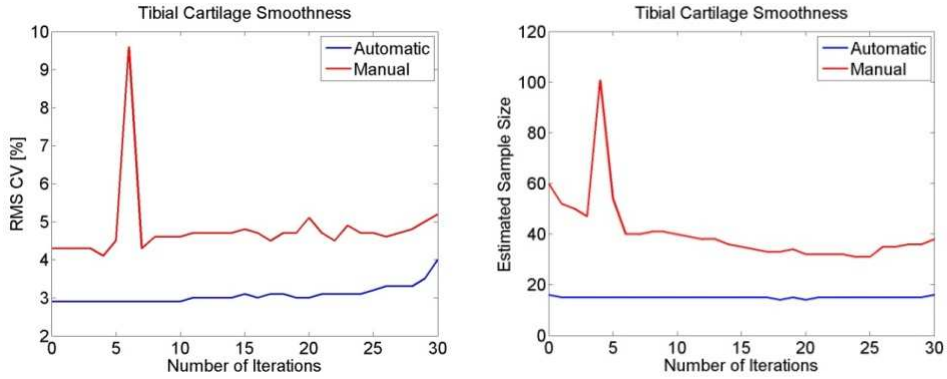

Figure 2.3: Variation of RMS CV (left) and ESS (right) for Manual and Automatic Segmentations from iteration 0 to 30 in case of Tibial.

The tibial smoothness marker based on automatic segmentations provides robust performance over a long range of iterations. The manual segmentation markers reveal worse performance and are less robust (low performance spikes). The performance graphs for the other scores (AUC and OR) and for the femoral smoothness markers (not illustrated) reveal similar patterns - also for the femoral sub-compartments. Inspired by these graphs, we fix the iteration number to 20. After more iterations, the performance decreases. At fewer iterations, the manual segmentation markers are less robust. Inspection of surface evolution visualizations (not shown) also reveals that this flow regularizes voxellation effects away without apparent shape deformation.

2.8 Results

For perspective, we evaluated the diagnostic performance of volume markers for the medial tibial and femoral compartments. The tibial volume marker resulted in RMS CV 9.8%, p=0.01 with ESS 211, OR 2.7, and AUC 0.62. The femoral volume marker had RMS CV 7.8%, p=0.03, ESS 292, OR 2.1, and AUC 0.60. Thereby, both tibial and femoral volume markers allow separation of healthy and diseased for diagnosis of early ROA with

borderline statistical significance.
The diagnostic scores are given in Table 2.1 for smoothness markers based on manual and automatic segmentations. The markers from manual segmentations allow highly significant diagnostic separation. Focusing on precision and sample size, the tibial and central femoral sub-compartments appear to have highest diagnostic power.
The smoothness markers from automatic segmentations allow even clearer diagnostic separation, superior to the markers based on manual segmentations. Again, the tibial and central femoral sub-compartments demonstrate best performance with precision 3.0% and sample size as low as 14 and 12, respectively.

Table 2.1: Diagnostic scores from smoothness measurements based on manual and automatic segmentations at 20 iterations. Com: Compartment, T: Tibial, F: Femoral, FA: Femoral Anterior, FC: Femoral Central, FP: Femoral Posterior.

	Manual					Automatic				
Com	CV	p	ESS	OR	AUC	CV	p	ESS	OR	AUC
T	5.1%	$2e^{-7}$	32	4.4****	0.76****	3.0%	$1e^{-8}$	14	8.8****	0.86****
F	3.5%	$3e^{-7}$	32	4.5****	0.74****	3.1%	$9e^{-13}$	14	15.8****	0.88****
FA	8.7%	$2e^{-4}$	55	5.5****	0.75****	8.0%	$1e^{-6}$	31	11.6****	0.80***
FC	4.0%	$1e^{-7}$	35	3.7***	0.73****	3.0%	$7e^{-16}$	12	11.6****	0.88****
FP	4.4%	$2e^{-5}$	52	1.8*	0.68***	4.4%	$4e^{-6}$	50	8.8****	0.78****

2.9 Conclusion

For many imaging biomarker tasks, the automated methods strive to match the performance that radiologists have achieved through years of experience. However, as we have exemplified with the smoothness markers, for some biomarkers a human observer will not be able to provide a direct, quantitative score. Even in the case where human annotations are used as the foundation for the actual quantification, the bias introduced by the annotation mechanism may influence the results negatively. For smoothness quantifications, manual segmentations performed by slice-wise outlining definitely introduce un-wanted artifacts: In each slice they typically look smooth whereas the surface implied across slices will be jagged. Rather than designing quantification methods that handles such artifacts, it may

be more fruitful to design fully automatic biomarkers that avoid the operator input bias/artifacts.

Furthermore, the evaluation reveals that the strongest diagnostic smoothness information is in the tibial and the central femoral regions. This corresponds to the central load-bearing regions, which seems highly plausible. Validation may appear more problematic for markers where no meaningful golden standard measurements are available. However, for biomarker to be used in a clinical setting, the most important evaluation should anyway be focused on the clinical task rather than technical measurement validation scores. Specifically, for markers to be used in clinical studies, a natural evaluation measure may be the sample size required in the study when using the marker. This can be estimated from existing study data - as done for the diagnostic smoothness marker we evaluated in this paper.

The evaluation of the smoothness marker showed that the fully automatic marker performed better than a smoothness marker based on manual segmentations and better than an alternative marker measuring cartilage volume. The potential future implications are better and earlier OA diagnosis as well as radiologist relief.

Chapter 3

Smoothness ability for cross-sectional separation of KL 0 & KL > 0 and KL ≤ 1 & KL > 1 is presented.

Tibial and Femoral Cartilage Smoothness: Diagnostic markers of early OA?

Tummala S, Karsdal MA, Bay-Jensen AC, Dam EB
This chapter is based on the abstract that was presented at OARSI 2009, Montreal, Canada

3.1 Purpose

One very early event in the initiation of osteoarthritis may be joint malalignment. Secondary to that, small alterations in the cartilage surface

(loss of smoothness) may signify early events leading to impaired cartilage integrity - prior to cartilage loss evaluated by volume. We investigated whether quantification of cartilage surface smoothness measured from magnetic resonance imaging (MRI) could provide a diagnostic marker of early stage radiographic OA (ROA).

3.2 Methods

The 21-month longitudinal study included 159 subjects prospectively selected as representative for the general population with age 21-81(mean 56), BMI 19-38 (mean 26), 48% female, and 51% knees with ROA (Kellgren and Lawrence, KL?1) at baseline (BL). KL was determined from radiographs acquired in a load-bearing semi-flexed position using the SynaFlex (Synarc). MRI scans with near-isotropic voxels were acquired from a Turbo 3D T1 sequence from a 0.18T Esaote scanner (40^0 FA, TR 50ms, TE 16 ms, scan time 10 minutes, resolution 0.7mm x 0.7mm x 0.8mm) and tibial and femoral medial compartments were segmented using a fully automatic computer-based voxel classification framework in the medial compartments. Smoothness was quantified by a curve-evolution framework after voxel super-sampling. Smoothness and volume scores were computed for full tibial and femoral compartments, and for sub-regions defining the anterior/central/posterior femoral sub-compartments.
The diagnostic abilities for splitting KL 0 vs. KL > 0 and KL ≤ 1 vs. KL > 1 were evaluated by T-test P-value (p), estimated required sample size (ESS), odd's ratio (OR), and area under the ROC (AUC). The scan-rescan precision was calculated by evaluating the Coefficient of Variation (RMS CV).

3.3 Results

The smoothness results are listed in the table. For smoothness, the scores were clearly different between healthy and ROA subjects ($p < 0.0001$) with the best diagnostic ability for separating KL ≤ 1 vs. KL > 1 in general and in particular in the central compartments.

Volume had CV of 6.6/7.0 % in the tibial/femoral compartments and showed borderline ability for separating the groups ($p < 0.05$) in some compartments with the femoral central compartment showing most promising scores of all compartments (p=0.01, ESS 388, OR 2.0, AUC 0.59).

Table 3.1: Diagnostic scores from smoothness measurements to separate A: KL 0 & KL > 0, B: KL ≤ 1 & KL > 1. Com: Compartment, T: Tibial, F: Femoral, FA: Femoral Anterior, FC: Femoral Central, FP: Femoral Posterior. *p < 0.05, **p < 0.01, ***p < 0.001, ****p < 0.0001.

		KL 0 & KL > 0				KL ≤ 1 & KL > 1			
Com	CV	p	ESS	OR	AUC	p	ESS	OR	AUC
T	2.8%	$2e^{-6}$	107	3.0**	0.64**	$4e^{-16}$	28	7.5****	0.78****
F	1.8%	$2e^{-8}$	74	3.1**	0.67**	$1e^{-18}$	29	11.1****	0.78****
FA	4.9%	$1e^{-3}$	226	2.0*	0.62**	$2e^{-4}$	119	2.7**	0.66***
FC	2.3%	$8e^{-8}$	82	3.1**	0.65**	$6e^{-19}$	26	10.6****	0.78****
FP	2.3%	$8e^{-6}$	120	2.8**	0.66**	$8e^{-11}$	66	5.9****	0.72****

3.4 Conclusion

The pathogenesis of OA is inhomogeneous. However, the later stages all lead to the same outcome; cartilage surface alteration, cartilage loss and eventually joint replacement. Following biochemical changes in the cartilage matrix, that may be induced by an array of traumatic or metabolic insults, fibrillation and focal lesions will likely lead to loss of cartilage surface smoothness at earlier stages of OA prior to general cartilage loss and joint space narrowing. The challenge is to measure this smoothness loss from the limited resolution of MRI (in particular low-field MRI).
The results indicated that smoothness estimates may indeed be indicative of early stage OA. The fact that a clearer separation was shown for KL ≤ 1 vs. KL > 1 could correspond with the pathogenesis chain of events suggested above. Furthermore, the clearest separation was observed in the tibial and the central femoral regions - this could suggest that the observed smoothness loss is linked to effects of load-bearing.

Chapter 4

Smoothness ability for diagnosis of OA is presented for different MTF compartments and also contrasted with conventional markers JSW and cartilage volume. Main results are in Figure 4.2 and Table 4.3, 4.4, 4.5.

Diagnosis of OA by cartilage surface smoothness quantified automatically from knee MRI

Tummala S, Bay-Jensen AC, Karsdal MA, Dam EB
This chapter is based on the article published in Cartilage 2011.

Objective: We investigated whether surface smoothness of articular cartilage in the medial tibio-femoral compartment quantified from magnetic resonance imaging (MRI) could be appropriate as a diagnostic marker of osteoarthritis (OA).
Method: At baseline, 159 community-based subjects aged 21 to 81 with

normal or OA-affected knees were recruited to provide a broad range of OA states. Smoothness was quantified using an automatic framework from low-field MRI in the tibial, femoral, and femoral sub-compartments. Diagnostic ability of smoothness was evaluated by comparison with conventional OA markers, specifically cartilage volume from MRI, joint space width (JSW) from radiographs, and pain scores.
Results: A total of 140 subjects concluded the 21-month study. Cartilage smoothness provided diagnostic ability in all compartments ($P < 0.0001$). The diagnostic smoothness markers performed at least similar to JSW and were superior to volume markers (e.g., the AUC for femoral smoothness of 0.80 was higher than the 0.57 for volume, $P < 0.0001$, and marginally higher than 0.73 for JSW, $P = 0.25$). The smoothness markers allowed diagnostic detection of pain presence ($P < 0.05$) and showed some correlation with pain severity (e.g., $r = -0.32$). The longitudinal change in smoothness was correlated with cartilage loss (r up to 0.60, $P < 0.0001$ in all compartments).
Conclusions: This study demonstrated the potential of cartilage smoothness markers for diagnosis of moderate radiographic OA. Furthermore, correlations between smoothness and pain values and smoothness loss and cartilage loss supported a link to progression of OA. Thereby, smoothness markers may allow detection and monitoring of OA-supplemented currently accepted markers.

4.1 Introduction

Osteoarthritis (OA) is one of the leading causes of pain and chronic disability worldwide due to deteriorating cartilage integrity and loss of articular cartilage, as well as changes in the underlying subchondral bone [38]. Clinically, it would be important to develop a treatment which if applied at the early stages of the OA might prevent the disease progressing to painful and disabling stages. A prerequisite for developing such a therapy - the first disease-modifying drug for OA (DMOAD) - is the identification of a mode of action which modifies the structure of cartilage and possibly the underlying bone. Such a drug development program would also require a clinical trial design that monitored disease progression. However, this is problematic as progression of OA in some clinical settings has been

absent [10,14,47,89]. This has initiated a discussion on which clinical phenotypes could allow for progression in clinical settings, and whether these subtypes would only respond to one specific type of intervention. Identification of common denominators for OA progression will be important. Several attempts have been made to identify the underlying causes and risk factors for progression in OA, including by the European TREATOA consortium [97] and the American Osteoarthritis Initiative [35,70]. Body Mass Index (BMI), subchondral bone turnover, misalignment, and meniscectomy are among the currently accepted risk factors for progression of OA [1,57]. However, the variation in these factors has served to spur further discussion on whether OA may indeed be a heterogeneous disease with a common end stage characterized by progressive cartilage loss and joint failure. This poses the question whether; independent of demographics, quantitative techniques may identify common parameters of cartilage biology and phenotype with a high risk progression. This would eliminate the need for segregation of patients into individual subtypes of OA. Such quantitative biomarkers may be highly important for clinical trial design. Several frameworks for characterization of biomarkers have been proposed. Recently, the BIPED categorization (Burden of disease, Investigatory, Prognostic, Efficacy of intervention and Diagnostic) has aided in understanding the individual potential of different markers [6].

The current requirement for acceptance of a DMOAD is to demonstrate efficacy in terms of joint space width (JSW) measured from radiographs, and joint function investigated by questionnaires (such as the WOMAC scale [8]. Selection criteria could typically be based on Kellgren and Lawrence score [60] (KL) and age - e.g. KL 2 or 3 and age 50-70 years. This poses potential disadvantages. Firstly, as selection currently is based on radiographs, this implies that subtle difference in cartilage pathology may not be accounted for as cartilage is not visible on radiographs. Secondly, studies may be designed to follow patients at relatively later stages of OA, as inclusion criteria are done by radiograph analysis in which bone sclerosis and osteophytes are evaluated. Since the later stages of OA are quite likely irreversible [82], new treatments focused at the earlier stages may have a higher chance of preventing progression or even curing the disease [7]. Novel biomarkers may aid in the identification and assessment

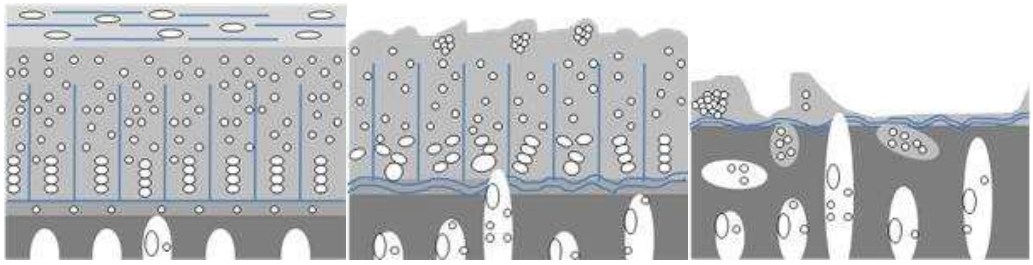

Figure 4.1: In early osteoarthritis, loss of the interior cartilage structure and loss of surface integrity occur before cartilage loss, sclerosis of underlying bone, and joint space narrowing.

of interventions in early OA.
Some of the central processes during the early stages of OA are illustrated in Figure 4.1. Healthy cartilage has a smooth lubricated surface (i.e. the superficial layer) (Figure 4.1A). The superficial layer is lost in early OA and the upper articular cartilage layer is exposed, which results in surface irregularities such as deamination, fibrillation, fissures, and erosions (Figure 4.1B). These irregularities can be detected by arthroscopy; but not by radiographs. As OA progresses to later stages, erosions become deep and sclerosis is observed (Figure 4.1C). It is at this stage that OA can be detected by radiographs as joint space narrowing (JSN) [7, 81]. It would be of high value to be able to measure the early surface irregularities and thereby identifying and treating OA at a stage where there is still articular cartilage left.

Radiographs may be well suited for capturing late-stage JSN and the associated bone phenotype. However, magnetic resonance imaging (MRI) allows direct visualization of articular cartilage in 3D [43]. Quantification of cartilage from MRI is required particularly when diagnosing middle-aged patients with medial pain, as radiographs do not show any remarkable changes in JSW [56]. The cartilage volume and thickness are the typical OA markers quantified from MRI. Knee cartilage volume declines at a faster rate with increasing age, as revealed in a longitudinal study [18, 37]. Mean cartilage thickness change of -0.5% was observed in the medial tibial cartilage in a one year longitudinal study using the Osteoarthritis Initiative data [36]. In the present study, we investigated whether quantification of the surface smoothness of articular cartilage may provide candidate

markers for clinical studies targeting early OA. Cartilage smoothness was estimated in the medial tibial and femoral knee compartments by a fully automatic computer-based method using MRI scans. The methods estimated the cartilage surface curvature at the smallest, effective spatial scale, implicitly limited by the MRI voxel size. We evaluated the diagnostic ability of cartilage surface smoothness against the status of radiographic OA as assessed by KL score. We compared with efficacy markers, JSN, which is currently accepted as a surrogate marker of joint replacement surgery, and loss of cartilage volume.

4.2 Materials and Methods

4.2.1 Study Population

The community-based baseline population of 159 subjects for the longitudinal study was selected such that it had even distributions of age, gender, BMI and varying degrees of OA symptoms. Subjects with inflammatory arthritis, any contraindication for MRI examination, or previous knee joint replacement were excluded from the study. The range of the time between baseline and follow-up visits was 15 to 21 months with mean time of 18 months.

4.2.2 Image acquisition

A total of 318 MRI scans of both knees were taken at baseline from the 159 subjects. Five out of 318 scans were removed from the study due to insufficient image quality in either MRI or X-ray, which left out 313 scans at baseline for the study. Thirty-seven images were rescanned 1 week later to evaluate scan-rescan precision.
Digital X-rays of both knees were acquired simultaneously in posterior-anterior position for every subject using SynaFlex from Synarc and the KL index was determined for each medial tibio-femoral joint. The 3D images of the knee were acquired using an Esaote C-span 0.18T scanner specifically developed for depicting the extremities with a scan time of approximately 10 minutes. The scanner parameters were as follows: 40^o flip angle, 50ms

repetition time and 16ms echo time. The voxel in-plane resolution was 0.7 mm x 0.7 mm with slice thickness between 0.7 mm and 0.94 mm.

4.2.3 Manual and Automatic Cartilage Segmentation

For a subset of 114 scans from the above baseline 313 scans and for all the scans that were rescanned after 1 week, manual segmentations were performed by slice-wise outlining by an expert radiologist. The same radiologist also assessed the KL score and determined the JSW from radiographs. The radiologist had 6 years of experience in reading knee radiographs and MRI prior to the study.
The 3D MRI scans of the tibial and femoral cartilages were segmented using a fully automatic supervised learning technique in which each voxel was assigned a probability of being tibial cartilage or femoral cartilage or background based on prior knowledge using k Nearest Neighbors (kNN) classifiers [41]. The training of the classifier and feature selection used the manual segmentations for 25 representative scans selected from the baseline 313 scans. The selected features for the classifiers were the cartilage position, intensities and local geometric features based on Gaussian derivatives.

4.2.4 JSW and volume quantification

JSW was determined in mm from radiographs by the expert radiologist. The volume of the binary segmentations (includes tibial-femoral, tibial, femoral, femoral anterior, femoral central and femoral posterior) was quantified by counting the number of voxels in each segment and the volume of each voxel in mm^3. The measured JSW and quantified cartilage volume values were normalized by the width of the knee. The JSN was quantified as the difference in JSW at baseline and follow-up.

4.2.5 Smoothness Quantification

Intuitively, a 'smooth' cartilage surface is free from irregularities, lesions and protrusions. We estimated the smoothness of the cartilage as the inverse of the fine-scale local mean curvature. The mean curvature is the

mean of the minimum and maximum curvatures. The smoothness of a compartment was computed as the mean local smoothness over the entire articular cartilage surface facing the synovium (disregarding the surface bone-cartilage interface).
The surface curvatures were quantified from either the manual or automatic cartilage segmentations. Before curvature evaluation, we regularized the cartilage segmentations, represented as binary volumes, to avoid voxellation effects by super-sampling them followed by Gaussian blurring and finally by mean curvature flow. As the flow progresses the cartilage surface with higher curvature values moves towards lower curvatures. From the curvature map the smoothness is then measured on the superior and inferior surfaces for the tibial and femoral compartments respectively. This basic methodology was previously described and evaluated as a diagnostic marker in the tibial compartment [39, 40].
The key parameters in the automatic curvature quantification methods were super-sampling factor, Gaussian blurring, step size, and the number of iterations in the curvature flow. Most important among these is the number of curvature flow iterations that defines the regularization needed to avoid voxellation effects while still retaining the ability to quantify fine-scale curvature. The performance of the method has been shown to be insensitive to the choice of number of iterations for a very large parameter interval. For additional details on the choice of parameters, see [92].

4.2.6 Cartilage Compartments

We focused the analysis on the medial compartments because OA is typically observed there [29, 66]. The femoral compartment was divided into anterior, central, and posterior sub-compartments. The femoral compartment was divided into sub-compartments to examine if the load-bearing and non-load regions of the compartment had different diagnostic ability compared to the whole femoral compartment. The division was based on the anterior-posterior width of the femoral compartment, which was divided into three thirds. The first third was denoted as posterior femoral sub-compartment. The central femoral sub-compartment included the area between the first to last third, and the last third was denoted as the anterior femoral sub-compartment. The splitting of femoral cartilage into sub-

compartments was validated to be sensible and robust by visual inspection on several scans, including healthy and diseased. The medial tibio-femoral joint with the tibial compartment and femoral sub-compartments is shown in Figure 2.2.

4.2.7 Statistical Analysis

We evaluated the marker precision by the root mean squared coefficient of variation (RMS CV) on markers quantified on the scan pairs acquired with one week in-between at baseline.
To avoid assumptions on the distributions of the markers, we evaluated the diagnostic performance using both parametric and non-parametric methods. We evaluated the p-value from an un-paired t-test (p) and the corresponding required estimated sample size (ESS) derived from power analysis at a significance level of 0.05 and power 0.8 [61]. We further evaluated the diagnostic separation of sub-populations by the area under the receiver-operator-characteristics curve (AUC). The Delong's nonparametric approach was used to test the statistical significance of AUC values [30]. The responsiveness of the markers was calculated as standardized response means (SRM) both in cross-sectional and longitudinal cases.
The potential appropriateness of an efficacy marker was investigated by the linear correlation coefficient. It was quantified between the yearly change in the smoothness marker and the yearly change in either JSW or cartilage volume. These were computed as follow-up minus baseline scores, divided by the duration of the interval in between.
The diagnostic performance of the smoothness scores from manual and automatic segmentations were compared using the above statistical analysis including RMS CV, p, ESS, and AUC.

4.3 Results

The study population statistics are given in Table 4.1 by age, body mass index (BMI), gender, and distribution across degrees of radiographic OA. Out of these subjects, 140 concluded the longitudinal study and contributed 270 scans at follow-up.

Table 4.1: Description of the study population with scan count, listing minimum-maximum (mean) values of age, Body Mass Index (BMI), gender and the distribution across the degrees of OA given by the KL Index (0 to 4).

	Baseline	Follow-up	Rescanned
Knee Count	313	270	37
Age	21-81 (56)	23-83 (58)	22-72 (55)
BMI(kg/m^2)	18-38 (26)	18-36 (26)	19-33 (26)
KL Index	0:158	0:139	0:11
	1:94	1:85	1:15
	2:31	2:24	2:3
	3:29	3:21	3:8
	4:1	4:1	4:0

4.3.1 Marker precision

The precision of each of the markers (volume, smoothness, and JSW) in each compartment quantified as RMS CV are shown in Table 4.2. Smoothness had equal or improved precision compared to volume for all compartments.

Table 4.2: The RMS CV, mean and standard deviation (SD) values for the markers joint space width JSW, volume, and smoothness in each medial compartment are given. The compartments are given as tibio-femoral (TF), tibial (T), femoral (F), femoral anterior (FA), femoral central (FC), and femoral posterior (FP).

	JSW(mm)		Volume(mm^3)		Smoothness(mm)	
Compartment	Mean ±SD	CV	Mean ±SD	CV	Mean ±SD	CV
TF	3.7 ±1.2	3.5%	6910 ±1457	5.2%	2.7 ±0.17	2.1%
T			2070 ±454	6.6%	2.8 ±0.22	3.2%
F			4840 ±1075	7.0%	2.8 ±0.22	2.7%
FA			889 ±276	17.1%	2.3 ±0.21	7.6%
FC			1590 ±394	7.2%	2.8 ±0.24	3.0%
FP			1903 ±476	15.4%	2.8 ±0.21	4.1%

4.3.2 Smoothness as Diagnostic marker of OA

The accuracy of the smoothness marker for separating the population into healthy subjects, with a KL ≤ 1, or those with OA as determined by a KL > 1, compared with the conventional markers, JSW and cartilage volume, is shown in Table 4.3. JSW allowed diagnostic separation ($p < 0.0001$, AUC 0.73) whereas cartilage volume allowing separation best in

the central femoral compartment ($p < 0.0001$, AUC 0.65). The smoothness markers were superior to both JSW and cartilage volume in all compartments, in particular in the tibio-femoral compartment ($p < 0.0001$, AUC 0.82) and the central femoral compartment ($p < 0.0001$, AUC 0.79). The increased performance of the smoothness markers compared to volume was statistically significant (e.g. the AUC for tibial smoothness of 0.79 was higher than 0.60 for volume, $p < 0.0001$). The cross-sectional SRMs for the JSW/volume/smoothness markers were -1.0/-0.35/-1.30 in the tibio-femoral compartment.

Table 4.3: Diagnostic scores for joint space width (JSW), cartilage volume, and smoothness quantified in the medial compartment for separating KL ≤ 1 and KL > 1 sub-populations. The compartments are given as tibio-femoral (TF), tibial (T), femoral (F), femoral anterior (FA), femoral central (FC), and femoral posterior (FP). Statistically significant differences are shown as * for $p < 0.05$, ** for $p < 0.01$, *** for $p < 0.001$, **** for $p < 0.0001$.

	JSW(mm)			Volume(mm^3)			Smoothness(mm)		
Compartment	p	ESS	AUC	p	ESS	AUC	p	ESS	AUC
TF	$2e^{-15}$	40	0.73**** (0.61-0.80)	0.01	280	0.58 (0.48-0.65)	$3\ e^{-35}$	19	0.82**** (0.75-0.86)
T				0.008	231	0.60* (0.51 - 0.66)	$7e^{-16}$	26	(0.71-0.85) (0.71-0.85)
F				0.02	362	0.57 (0.47-0.67)	$5e^{-25}$	23	0.80**** (0.70-0.85)
FA				0.6	6490	0.52 (0.43-0.58)	$3e^{-8}$	50	0.72**** (0.65-0.77)
FC				$5e^{-5}$	111	0.65** (0.55-0.74)	$4e^{-28}$	23	0.79**** (0.72-0.86)
FP				0.23	1438	0.51 (0.42-0.58)	2^{e-14}	40	0.76**** (0.67-0.84)

The potentiality of the smoothness marker in diagnosing different degrees of radiographic OA, indicated by KL score, is illustrated for the tibial (in Figure 4.4A) and femoral (Figure 4.4B) compartments. The smoothness marker allowed cross-sectional separation of KL levels above 1.

4.3.3 Smoothness as Efficacy Marker

The longitudinal changes in smoothness were correlated with the change in volume for each compartment. These correlations are shown in Table 4.4. For all compartments, loss of smoothness was significantly correlated to volume loss, but not to JSN. The strongest correlation was 0.64

between smoothness loss and volume loss in the posterior medial femoral compartment. The longitudinal SRMs are 0.14/-0.10/-0.30 for JSN/cartilage loss/smoothness in the tibio-femoral compartment.

Table 4.4: The linear correlations between change in cartilage surface smoothness and JSN and cartilage volume loss for each compartment. The compartments are given as tibio-femoral (TF), tibial (T), femoral (F), femoral anterior (FA), femoral central (FC), and femoral posterior (FP). Statistically significant differences are shown as * for $p < 0.05$, ** for $p < 0.01$, *** for $p < 0.001$, **** for $p < 0.0001$.

Compartment	Smoothness change vs. JSN	Smoothness change vs. volume loss
TF	0.01	0.31****
T	-0.07	0.26****
F	0.10	0.43****
FA	0.09	0.22***
FC	0.06	0.30****
FP	0.05	0.60****

4.3.4 Smoothness quantification from manual and automatic segmentations

The diagnostic performance of the smoothness markers evaluated on the subset of 114 scans, in which both manual and automatic segmentations were available, is shown in Table 4.5. The smoothness markers allowed diagnostic separation of the healthy and diseased (defined by KL ≤ 1 or KL > 1 respectively) sub-populations regardless of whether the quantification was based on manual or automatic segmentations. For all compartments and all performance criteria, the performance of the markers based on automatic segmentations was equal to or higher than those based on manual segmentations.

4.4 Discussion

Loss of smoothness may be a common, early denominator for the heterogeneous paths leading to cartilage degeneration, and may in addition capture the roughening of the surface that is associated with increased disease progression. The presented cartilage smoothness marker may biologically be understood as targeting an early to medium stage of OA.

Table 4.5: Diagnostic scores for cartilage smoothness quantifications in the medial compartments based on manual and automatic segmentations for a subset of 114 scans. The compartments are given as tibio-femoral (TF), tibial (T), femoral (F), femoral anterior (FA), femoral central (FC), and femoral posterior (FP). Statistically significant differences are shown as * for $p < 0.05$, ** for $p < 0.01$, *** for $p < 0.001$, **** for $p < 0.0001$.

	Manual				Automatic			
Compartment	CV	p	ESS	AUC	CV	p	ESS	AUC
TF	3.1%	$1e^{-8}$	26	0.78**** (0.54 - 0.85)	2.1%	$1e^{-16}$	10	0.90**** (0.83 - 0.95)
T	5.1%	$1e^{-6}$	37	0.76**** (0.64 - 0.85)	3.0%	$8e^{-12}$	14	0.87**** (0.77 - 0.95)
F	3.5%	$7e^{-7}$	34	0.75*** (0.64 - 0.88)	2.9%	$4e^{-14}$	13	0.88**** (0.77 - 0.93)
FA	8.7%	$5e^{-5}$	42	0.76**** (0.64 - 0.84)	8.0%	$1e^{-7}$	28	0.80**** (0.71 - 0.91)
FC	4.0%	$4e^{-7}$	36	0.73*** (0.59 - 0.81)	3.1%	$9e^{-16}$	11	0.88**** (0.80 - 0.95)
FP	4.4%	$8e^{-5}$	57	0.68** (0.54 - 0.80)	4.4%	$6e^{-8}$	31	0.80**** (0.71 - 0.87)

Importantly, whereas a histological assessment focuses on local cartilaginous pathologies, the present computation provides a representation of the degree of pathology in the knee cartilage overall. The earlier stages of OA may be appropriate to evaluate the efficacy of many of the current treatment development projects. Thus, the present data may have important implications for clinical trial design.

Early cartilage damage is associated with extensive activities of proteases within the articular cartilage such as matrix metallo proteases (MMPs) and aggrecanases [88]. These enzymes are currently the target of many treatment strategies, and consequently may best be evaluated in a selected OA population in which cartilage is still present and can be treated, rather than in the later stages of OA where cartilage is lacking [57]. We suggest that the present technology may be suited for short-term proof of concept studies for selected treatments targeting the mild stages of OA.

Although many approaches to measure cartilage quantity from MRIs have been published, the literature contains few attempts to quantify cartilage quality from its surface curvature. Large scale curvature analyses were performed both by Hohe et al [49] and Terukina et al [96] on the cartilage surface shown by MRI. However, these large scale measurements were re-

lated to joint congruity rather than smoothness. Efforts have been made to evaluate surface roughness from ultrasound by Chiang et al [20] and most recently by Kaleva et al [55]. The surface roughness index was estimated acoustically for diagnosis of early OA. Ateshian et al [5] used stereophotogrammetry to collect data from human thumb carpometacarpal joints, and curvature maps were calculated by taking the inverse of the osculating circle fitted at every surface point. However, due to the invasiveness, these methods are not feasible for clinical practice or for clinical studies. The smoothness marker used in the current study relies on fully automated quantification from non-invasive low-field MRI.

The non-invasiveness of the MRI-based smoothness quantification complicates a physical validation of the estimated surface curvatures. In the present study, a physical validation of cartilage quality, for instance, by histology, would have been impractical in such a large general population of subjects. In addition, low-field MRI has been validated less than high-field MRI for cartilage morphometry. The main limitations of low-field MRI are a low signal-to-noise ratio and a low spatial-temporal resolution compared with high-field MRI. However, low-field MRI has advantages of low costs for installation, scanning and maintenance, and in some settings, low-field MRI has the potential to reduce overall cost with little loss of diagnostic performance [46]. This is of interest for large clinical studies.

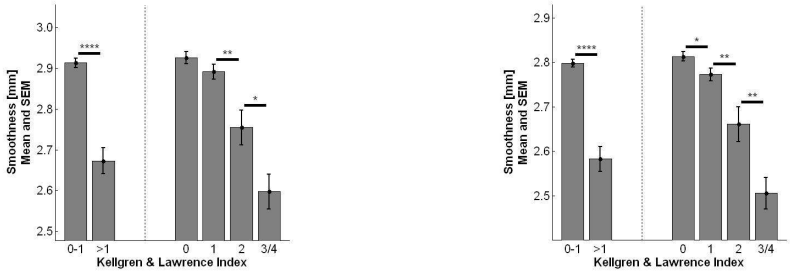

Figure 4.2: The smoothness markers at each level of OA for the tibial (3A) and femoral (3B) compartments. The mean smoothness score is given with standard error of the mean given as error bars. The KL ≤ 1 and KL > 1 sub-populations are compared to the left of the dashed lines. To the right, the scores are given for each level of KL. Statistically significant differences are shown as * for $p < 0.05$, ** for $p < 0.01$, *** for $p < 0.001$, **** for $p < 0.0001$.

The lack of physical validation of both the imaging modality and the smoothness markers limits the strength of the results. In particular, the smoothness quantification could be biased by segmentation artifacts not directly related to the desired pathologies (e.g. fibrillation). Previously, the accuracy of the smoothness quantification method was validated using digital phantoms [39]. Here, the evaluating comparing the quantifications based on manual and automatic segmentations was performed to investigate this. The fundamentally different nature of slice-wise 2D manual outlining and 3D automatic segmentation creates fundamentally different segmentation artifacts. The fact that similar results were obtained based on these two segmentation sources indicate that the smoothness quantifications are indeed given by the cartilage surface rather than segmentation artifacts. The RMS CVs of 4.6%-5.8% between automatic and manual baseline smoothness values in all the compartments supports that the estimated values are due to smoothness and not due to algorithmic artifacts. Interestingly, the smoothness markers quantified from the computer-based automatic segmentations performed better than those based on the manual segmentations. We attribute this to the between-slice artifacts that arise from manual, slice-wise outlining. While each slice typically looks smooth, a 3D visualization will reveal jagged edges from slice to slice. The finding demonstrates that for some markers, like surface smoothness, operator artifacts can be avoided by automatic methods. However, even in the light of these positive validation results, a physical validation would be desirable. In the present study, the smoothness markers demonstrated promising results. The precision of the smoothness markers in all compartments - tibial, femoral, and femoral sub-compartments - was equal to or superior to that of the volume markers. For most compartments, the smoothness RMS CV scores were around 3% (see Table 4.2). The smoothness markers also allowed diagnostic separation of healthy and early OA in all compartments with AUC scores between 0.72 and 0.82. These scores were superior to the cartilage volume scores for reliably diagnosing OA by KL score (e.g. the AUC for femoral smoothness of 0.80 was higher than 0.57 for volume, $p < 0.0001$). A comparison with the diagnostic performance of JSW is less interesting since JSW is a criterion in defining the KL score. As Figure 3 illustrates, in addition to the diagnostic separation between healthy knees

and those with the higher KL scores, the smoothness markers also allow separation at later stages of OA.

Finally, the results demonstrated that longitudinal progression in smoothness was related to longitudinal cartilage loss (see Table 4.4). For instance, the correlation coefficient calculated for yearly change in smoothness versus volume (0.41) in the femoral compartment showed a strong relation ($p < 0.0001$). These strong associations indicate that smoothness markers may be appropriate not only to measure cartilage quality at a given point of time, but may also be useful indicators of longitudinal disease progression, and thus could potentially become markers of efficacy in clinical studies of OA.

In general, we observed smoothness markers measured in the tibial and central femoral compartments, which are also the most load-bearing compartments, were the most reliable indicators of the presence of OA. This supports an intuitive reasonable relationship between biomechanical stress and initiation of OA. In conclusion, cartilage surface smoothness quantified automatically from MRI may provide suitable diagnostic of the mild OA with utility in future clinical studies.

Chapter 5

Novel methods for Tibio-femoral contact area and congruity index quantification are proposed. Main results are in Table 5.3, 5.4, 5.5 and Figure 5.5.

Automatic Quantification of Tibio-Femoral Contact Area and Congruity

Tummala S, Nielsen M, Lillholm M, Christiansen C, Dam EB
This chapter is based on the manuscript currently under re-review in IEEE Trans. Med. Imaging. Part of this was presented as a poster at MICCAI, CBM6 workshop and orally at OARSI 2011.

We present methods to quantify the medial tibio-femoral (MTF) joint contact area (CA) and congruity index (CI) from low-field magnetic resonance imaging (MRI). Firstly, based on the segmented MTF cartilage compartments, we computed the contact area using the Euclidian distance

transformation. The CA was defined as the area of the tibial superior surface and the femoral inferior surface that are less than a voxel width apart. Furthermore, the CI is computed point-by-point by assessing the first and second order general surface features over the contact area. Mathematically, it is the inverse distance between the local normal vectors (first order features) scaled by the local normal curvatures (second order features) along the local direction of principal knee motion in a local reference coordinate system formed by the directions of principal curvature and the surface normal vector. The OA-diagnositc abilities of the CA and the CI for various diagnotic tasks (disease severity was assessed using the Kellgren & Lawrence Index (KL)) were cross-validated on 288 knees at baseline. Longitudinal analysis was performed on 245 knees. The precision quantified on 31 scan-rescan pairs (RMS CV) for CA was 13.7% and for CI 7.5%. The CA increased with onset of the disease and then decreased with OA progression. The CI was highest in healthy and decreased with the onset of OA and further with disease progression. The CI showed an AUC of 0.69 ($p < 0.0001$) for separating KL 0 & KL > 0. For separating KL ≤ 1 & KL > 1 knees, the AUC for CI was 0.73 ($p < 0.0001$). The CA demonstrated longitudinal responsiveness (SRM) at all stages of OA, whereas the CI did so for advanced OA stages only. Eventually, the quantified CA and the CI might be suitable to help explaining OA onset, diagnosis of (early) OA, and measuring the efficacy of DMOADs in clinical trials.

5.1 Introduction

Musculoskeletal disorders are the most frequent form of chronic disabilities worldwide [15, 65]. They limit the individual's work ability causing pain and limited range of motion. Osteoarthritis (OA) is the most common type of arthritis and a prevalent musculoskeletal disorder in the elderly [64, 84]. OA mostly affects the major load-bearing joints in the body including knee, hip and foot [17]. Biomechanical factors play a vital role in the pathogenesis of OA [54]. One of the early biomechanical mechanisms in the initiation of knee OA is tibio-femoral malalignment [16]. It has been hypothesized that local incongruity of the articular surfaces may play a role in determining alignment [52].

The contact area in the medial tibio-femoral joint (MTF) is the region, where the articular cartilage surfaces that covers the ends of the bone are in close proximity. In the contact area, the two surfaces interact and transfer the local stresses effectively, and thereby cause no or insignificant degeneration to the cartilage in a healthy joint. In the following, we use contact area as the cartilage-cartilage contact area but not the cartilage-meniscus contact area. Furthermore, we use *contact area* when referring to the region of contact (close proximity) and CA as the area per se of the contact area.

The use of MRI is advancing rapidly in OA as it allows non-invasive visualization of the cartilage in 3D [43]. Studies have computed the CA in knee joints non-invasively using MRI [48, 80]. Moreover, in a recent study, the CA was different for healthy and OA knees; this was shown in an indirect manner for the MOST study using MRI [85].

The 'Congruity' could physically be defined as how well any two surfaces fit together. In a healthy MTF joint, the smooth femoral cartilage surface articulates well with the tibial cartilage surface and are congruent. In part, the congruency is stabilized by the meniscus. It was documented that incongruity may be a major factor in the onset of OA [49]. In [5], the carpometacarpal joint cartilage surfaces were reconstructed employing stereophotogrammetry and the incongruity was quantified from the principle curvatures and directions of the opposing surfaces at the point of contact to conclude that female joints were less congruent than male joints. The methods in [5] were used to compute the incongruity by constructing the cartilage surfaces by triangulation and to contrast it among different knee compartments using MRI [49]. In a recent study [22], the same type of approach was used to measure the incongruity in the patellofemoral joint. To our knowledge, no studies have been conducted that attempt to differentiate the local congruity of healthy and OA tibio-femoral joints from MRI.

The articular cartilage in the contact area is significantly thicker and facilitates the load distribution in a healthy joint [68]. Therefore, when the contact ares that normally transforms the local stresses is dislocated, the cartilage surfaces in the 'new' contact area may fail to adapt the functions of the cartilage surfaces in the normal contact area [2]. This incongruity may initiate a degradation of the cartilage surface smoothness and when

the two rough surfaces in contact are in motion relative to one another, more friction is induced which may in turn increase the degeneration and eventually lead to complete loss of cartilage.

In this paper, we propose methods to quantify the CA and the Congruity Index (CI) in the MTF joint. The CA is quantified using the Euclidean distance transform. Inside the contact area, the local normal vectors (first order features) and local normal curvatures (second order features) along the local direction of principal knee motion of the tibial and femoral surfaces are computed. We propose that the surfaces are congruent if the distance between the local normal vectors scaled by signed local normal curvature is very small (close to zero) over the CA. We validated the ability of the CA and the CI for cross-sectional separation of healthy, early, and advanced radiographic OA knees. The method we propose is fully automatic and computes the local congruity by matching the tibial and femoral cartilage surface asperities over the contact (limited by scan resolution).

The next section contains a description of our proposed methods for CA and CI quantification and application to the MTF joint. The third section explains the experimental setup. The fourth section presents the results that are discussed in the fifth section and conclusions are given in the final section.

5.2 Methods

We initially propose general formulas for modeling dynamic and static knee joint biomechanics. 'Dynamic' is in the sense of integrating the static joint biomechanics over all possible flexion angles. We focus on a simple model based on load, contact area, and congruity.

5.2.1 Dynamic joint biomechanics

We formulated the double integral below that models the biomechanics (DJB) as a function of flexion angle θ in a knee:

$$DJB = \iint L(p, \theta) * d_{cong}(fem(p), tib(fem(p), \theta))dpd\theta \tag{5.1}$$

Where $L(p, \theta)$ is the load in the contact area and p is a position in the cartilage. The function d_{cong} is the similarity measure in the contact area that computes the local congruity. The load is the contact stresses in the contact area and can be computed by modeling the knee joint using, e.g, finite element analysis [91].

In the present work, we mainly focussed on quantification of the local (point-by-point) congruity and therefore, one of the intial simplifications was setting the load at each point in contact area equal to one, expressed in equation 5.3.

$$L(p, \theta) = \begin{cases} 1 & \text{if } p \in contactarea \\ 0 & \text{otherwise} \end{cases} \tag{5.2}$$

One of the focuses of this paper is formulating and computing the function d_{cong} that computes the local congruity. We propose that two surfaces are mathematically congruent if they have the same first and second order features, i.e., same normal vectors and curvatures. We formulate the CA and CI for the general surfaces in contact as described in the following section.

5.2.2 Contact Area and Congruity Index formulation

Consider two surfaces $S_a : R^2 \rightarrow R^3$ and $S_b : R^2 \rightarrow R^3$ as shown in Fig. 5.1 where we would like to estimate their contact area and congruity index. Let S_a^c and S_b^c be the regions of S_a and S_b respectively that are in close proximity. Let X, Y and Z be the axes of a coordinate system.

The CA (between S_a and S_b) is the average of the area of S_a^c and area of S_b^c. The area of S_a^c can be computed by computing the area of its patch triangles. Similarly, the area of S_b^c. Therefore, the CA between S_a and S_b can be expressed as follows:

$$CA = \frac{area(S_a^c) + area(S_b^c)}{2} \tag{5.3}$$

The CA computation is detailed in section 5.2.3.

The normal vectors (first order features) at S_a^c and S_b^c are denoted as $\overline{n_a}$ and $\overline{n_b}$. The second order features are the curvatures. The maximal and minimal principal curvatures of the surface S_a^c are denoted as k_a^1 and

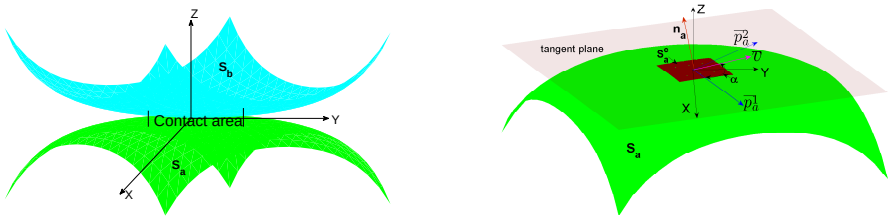

Figure 5.1: Showing two artificial surfaces in contact and illustration of how the normal vector and the principal curvatures are located in the contact region of S_a. The X, Y and Z axes form the global coordinate system. The tangent plane is perpendicular to the normal vector $\overline{n_a}$. The red zone S_a^c is the region where S_a and S_b are in contact. The $\overline{p_a^1}$ and $\overline{p_a^2}$ are the maximal and minimal principal directions respectively and $\overline{v}$ is the direction along which we computed the normal curvature. Angle α is the angle between $\overline{p_a^1}$ and $\overline{v}$.

k_a^2 respectively and the corresponding principal directions are $\overline{p_a^1}$ and $\overline{p_a^2}$. Similarly, the maximal and minimal principal curvatures of the surface S_b^c are denoted as k_b^1 and k_b^2 respectively and the corresponding principal directions are $\overline{p_b^1}$ and $\overline{p_b^2}$.

Consider an arbitrary direction $\overline{v}$ in the tangent plane (which is perpendicular to the normal vector as shown in Fig. 5.1) along which we would like to compute the curvature. This normal curvature on the sub-surface S_a^c in the direction of $\overline{v}$ can be computed by Euler's formula:

$$k_a^{\overline{v}} = k_a^1 cos^2\alpha + k_a^2 sin^2\alpha \tag{5.4}$$

where α is the angle between the maximal principal direction $\overline{p_a^1}$ and direction $\overline{v}$ along which the curvature is calculated.

Similarly, the normal curvature on the sub-surface S_b^c in the direction of $\overline{v}$ is

$$k_b^{\overline{v}} = k_b^1 cos^2\beta + k_b^2 sin^2\beta \tag{5.5}$$

where β is the angle between the maximal principal direction $\overline{p_b^1}$ and $\overline{v}$.

The *CI* was defined by combining the first and second order features of

S_a^c and S_b^c as given below.

$$d_{cong} = CI = \frac{1}{||k_a^{\overline{v}}\overline{n_a} - k_b^{\overline{v}}\overline{n_b}||} \tag{5.6}$$

Note: The norm in the denominator is Euclidean. For locally flat surfaces in contact, the curvatures are zero and therefore have infinite congruity because the denominator of equation 5.6 becomes zero and vice versa.

The CI computation is detailed in section 5.2.3.

5.2.3 Application to medial tibio-femoral joint

The MTF cartilage compartments of MRI knee scans (see details in Section 3) were segmented fully automatically using a voxel classification approach [39]. The CA and CI quantification steps are presented in detail below.

Regularization of MTF cartilage compartments

The binary segmentations were regularized using mean curvature flow in a level set formulation [86] to reduce the voxellation effects. The parameters in this flow are, step size (we fixed this parameter at 0.15 for the 3D case), scale at which the gaussian derivatives are computed and the number of iterations of the flow. Mathematically, it is formulated as:

$$\frac{\partial \phi}{\partial t} = k_M |\nabla \phi| = [\nabla(\frac{\nabla \phi}{|\nabla \phi|})]|\nabla \phi|, \tag{5.7}$$

where $\nabla\phi$ is the gradient (gaussian derivatives) of the level set representation ϕ and k_M is the mean curvature computed from derivatives of ϕ. We represented ϕ as a signed distance function to make the computations straightforward. We regularized the tibial and femoral cartilage compartments separately.

Contact area computation

The tibial and femoral cartilage contact areas were estimated by employing the Euclidean binary distance transform (DT). In this, a kd-tree implementation was used for faster computation. The tibial contact area *TibProx*

was located by estimating the coordinates (t) in the tibial cartilage surface, which were less than one voxel width (vw) away from the femoral cartilage surface; *TibProx* corresponds to S_a^c in the general formulation above. The femoral contact area *FemProx* (corresponding to S_b^c above) is similarly located by estimating coordinates (f) in the femoral cartilage surface that are less than one voxel width away from the tibial cartilage surface. These definitions are summarized in equations 5.8 and 5.9 below. As both cartilage surfaces are the result of voxel segmentations, locally they can be quite complex and thus the number of points in *TibProx* and *FemProx* may not be the same.

$$TibProx = \{t \in tib | DT(t, fem) < vw\} \tag{5.8}$$

$$FemProx = \{f \in fem | DT(f, tib) < vw\} \tag{5.9}$$

In equations 5.8 and 5.9, tib is the tibial cartilage and fem is the femoral cartilage.

The presence of cartilage defects/synovial fluid can lead to non-solid cartilage areas. Therefore, we smoothed *TibProx* and *FemProx* before computing the final areas. It involves Gaussian smoothing with a standard MATLAB function *smooth*3 using a Gaussian kernel with a standard deviation of 0.65 voxels and a kernel mask size of 3×3 voxels, and thus small noisy holes due to, e.g., synovial fluid very likely disappear. We validated this by visualizing randomly selected contact areas. The area of *TibProx* and *FemProx* respectively is then defined as the mean of the selected triangle faces of the smoothed patch surfaces (generated by using the MATLAB function *patch*). This was based on the upward vertex normal vectors for *TibProx* and the downward vertex normal vectors for *FemProx* and then computing the mean value of them.

Formalizing this, let *TibProx* have P_1 selected patch triangles and let V_1, V_2 and V_3 be the vertices of a triangle *tri*. The area of the triangle *tri* is then given by

$$A_{tri} = \frac{1}{2}\|(V_1 - V_2)X(V_1 - V_3)\| \tag{5.10}$$

and the area of *TibProx* is the sum of the area of all P_1 triangles

$$A_{TibProx} = \sum_{tri=1}^{P_1} A_{tri} \tag{5.11}$$

Similarly, $A_{FemProx}$ can be computed using equation 5.10 and 5.11. The CA per se was then estimated as the mean of the areas of *TibProx* and *FemProx*:

$$CA = \frac{A_{TibProx} + A_{FemProx}}{2} \tag{5.12}$$

Since the CA is a knee width dependent measure; we normalized the value using the tibial bone width (excluding osteophytes) to avoid a bias between large and small knees. The normalized CA is calculated as:

$$normalizedCA = \frac{CA}{TBW^2} \tag{5.13}$$

In the equation above, *TBW* is the letero-medial tibial bone width. The *TBW* was measured from anterior-posterior radiographs which made it impossible to assess the antero-posterior tibial bone length (*TBL*). We therefore normalized the CA with *TBW* squared instead of the, perhaps more natural, product of the *TBW* and *TBL*. The underlying simplification here is the assumption that the width length ratio is constant between knees. The normalized CAs were used for the validation below. Fig. 5.3 contains a visualization of the location of the CA in a healthy MTF joint.

Congruity computation

The local congruence of the tibio-femoral joint is calculated by assessing the first and second order features of the surface *TibProx* and *FemProx* point-by-point. If *TibProx* and *FemProx* are locally congruent, then the first and second order features will match well.

First order features Let $\overline{n_t}$ be the normal vector at a point t in the *TibProx* and $\overline{n_f}$ be the normal vector at the corresponding point f in the *FemProx*. Mathematically, these normal vectors are computed from first order partial derivatives of the level set representation: $\overline{n_t} = \frac{\nabla\phi_t}{|\nabla\phi_t|}$. Similarly, for $\overline{n_f}$.

Second order features The second order features are the curvatures as formulated in section B. We computed the normal curvature along the principal direction of motion instead of the mean of principal curvatures. Since the principal knee motion is flexion/extension, we approximated the local principal direction of motion as the cross product of a normal vector in the sagittal direction with the local normal vector. The normal curvature at a point t on *TibProx* in the direction $\overline{v}$ is computed using equation 5.4. Similarly, the normal curvature at a point f on *FemProx* in the direction $\overline{v}$ is computed by using equation 5.5. We will now see in detail how these normal curvatures are computed.

The Hessian H_T at a point t on the *TibProx* and the Hessian H_F at the corresponding point f on the *FemProx* are constructed using second order partial derivatives of ϕ_t and ϕ_f respectively:

$$H_T = \begin{pmatrix} \phi_{txx} & \phi_{txy} & \phi_{txz} \\ \phi_{txy} & \phi_{tyy} & \phi_{tyz} \\ \phi_{txz} & \phi_{tyz} & \phi_{tzz} \end{pmatrix}$$

$$H_F = \begin{pmatrix} \phi_{fxx} & \phi_{fxy} & \phi_{fxz} \\ \phi_{fxy} & \phi_{fyy} & \phi_{fyz} \\ \phi_{fxz} & \phi_{fyz} & \phi_{fzz} \end{pmatrix}$$

Since, we are interested in surface principal normal curvatures, the orthonormal basis for H_T and H_F are say b_t and b_f. The transformed/projected hessian matrices become, H_{Txy}= b_t^T*H_T*b_t and H_{Fxy}= b_f^T*H_F*b_f. The eigenvalues of H_{Txy} are divided with the gradient magnitude ($|\phi_t|$) and constitute the principal curvatures (k_t^1 k_t^2). The corresponding eigenvectors are the principal directions ($\overline{p_t^1}$ $\overline{p_t^2}$). Using equation 5.5, the normal curvature at t in the direction of $\overline{v}$ becomes, $k_t^{\overline{v}}$= $k_t^1 \cos^2\alpha + k_t^2 \sin^2\alpha$, where α= $\cos^{-1}(\overline{p_t^1} * \overline{v})$. Eventually, $k_t^{\overline{v}}$ simplifies to:

$$k_t^{\overline{v}} = k_t^1 + [(k_t^1 - k_t^2) * (\overline{p_t^1} * \overline{v})] \tag{5.14}$$

Similarly, the normal curvature at f on the *FemProx* in the direction of $\overline{v}$ is given by $k_f^{\overline{v}}$= $k_f^1 \cos^2\beta$ + $k_f^2 \sin^2\beta$ with β= $\cos^{-1}(\overline{p_f^1} * \overline{v})$. The simplified expression for $k_f^{\overline{v}}$ becomes,

Table 5.1: Contact area and Congruity Indices mean and SD values for KL 0, KL 1, KL 2, KL 3 subjects respectively for scan and rescanned knees. Fixed parameters were used (2.4mm curvature scale and 4 curvature flow iterations). N: number of knees

KL Index (N)	CA (mean ±SD)	CA rescan (mean ±SD)	CI (mean ±SD)	CI rescan (mean ±SD)
0 (11)	0.106 ±0.021	0.103 ±0.029	10.6 ±4.2	10.2 ±3.6
1 (13)	0.124 ±0.030	0.130 ±0.029	7.1 ±2.9	7.5 ±3.1
2 (2)	0.100 ±0.008	0.090 ±0.017	10.6 ±0.8	10.9 ±0.9
3 (5)	0.091 ±0.054	0.101 ±0.049	6.8 ±4.6	6.4 ±3.2

$$k_f^{\overline{v}} = k_f^1 + [(k_f^1 - k_f^2) * (\overline{p_f^1} * \overline{v})] \tag{5.15}$$

We computed the point-by-point congruity indices using equation 5.6 over the contact area.

As mentioned above, the segmented nature of the cartilage surfaces may mean that the number of points in *TibProx* and in *FemProx* are different. Due to this assymetry, the overall CI in the contace area is computed as the mean of the CI from the *TibProx* and the CI from the the *FemProx*. Let *TibProx* have N_1 points and *Femprox* has N_2 points. The final CI calculation is summarized as:

$$CI = \frac{\frac{\sum_{p=1}^{N_1} CI_p}{N_1} + \frac{\sum_{q=1}^{N_2} CI_q}{N_2}}{2} \tag{5.16}$$

where CI_p and CI_q are the congruity indices at the locations p and q.

If the surfaces are conforming locally, the curvatures signs are different and therefore one of the normal vectors flips and gives a close to zero distance. If more pairs are like this over CA we get a smaller distance if the tibio-femoral joint is locally more congruent.

The free parameters are the scale at which the curvatures are computed and the number of iteration in the mean curvature flow.

5.3 Experimental setup

All the computational work is carried out in MATLAB version 7.12 (The mathworks Inc.).

5.3.1 Study population

We validated the proposed quantifications of the CA and the CI on a 21-month longitudinal study population consisting of 159 subjects with age range 21-81 years (mean 56) and varying degrees of OA symptoms. Subjects with inflammatory arthritis, any contradiction for MRI examination, or previous knee joint replacement were excluded. MRI scans of all the subjects were acquired using a Turbo 3D T1 sequence from a 0.18T Esaote C-span scanner (40^0 flip angle, 50-ms repetition time, 16-ms echo time) with a scan time of approximately 10 minutes. The voxel in-plane resolution was 0.7mm x 0.7mm with average slice thickness of 0.8mm. The scans were acquired in the near full knee extension in supine position with no applied limb loading. The severity of OA was graded by an experienced radiologist from the radiographs based on the Kellgren & Lawrence index [60]. We have 288 knee scans at baseline (BL) for cross-sectional study design, 245 at BL as well as at follow-up for longitudinal study design. We also have 31 knees that were rescanned one week after the baseline visit for validating the quantification precision. The detailed study population was described in [**?**].

5.3.2 Statistical analysis

The precision of the quantification is computed as the root mean squared coefficient of variation (RMS CV) as well as linear correlation coefficient (CC). The diagnostic ability of the measurements to separate any two groups is calculated from the area under the ROC curve (AUC). The statistical significance of the AUC value is computed from the Delong-test [30]. The longitudinal responsiveness of the measure is quantified as standardized response mean (SRM). The SRM is measured as the ratio of mean change to the standard deviation of change between follow-up and baseline values.

5.3.3 Cross-validation

The ability of the CA and CI quantification methods is cross-validated for tasks of diagnosis that include cross-sectional separation of KL 0 & KL 1, KL 2 & KL 3/4, KL 0 & KL > 0 and KL ≤ 1 & KL > 1. We formulated the curvature scale and the number iterations in the curvature flow as $1.5^{n+1} * voxelsize$ and 2^n respectively where n is varying from one to four. Thereby, the measures are quantified for 16 combinations, which are constituted from the curvature scale (1.6 mm, 2.4 mm, 3.6 mm, and 5.4 mm) and the number of iterations (2, 4, 8, and 16).

The tasks are divided to facilitate the separation of healthy and early OA; the separation of KL 2 and above (generally used in clinical trials). The scans at BL are randomly divided into training and validation sub-sets. Using the training sub-set, the curvature scale and the number of iterations are optimized for the best AUC, and the optimized scale and iterations are used on validation sub-set to compute the validated AUC. The process is repeated for 100 times and the median values are reported.

5.4 Results

In this paper, the scores are computed at the scale (2.4 mm) and the iterations (4) corresponding to the maximum trained AUC of the tasks listed in Table 5.4 or 5.5. The CA and CI values for scan-rescan knees are given in

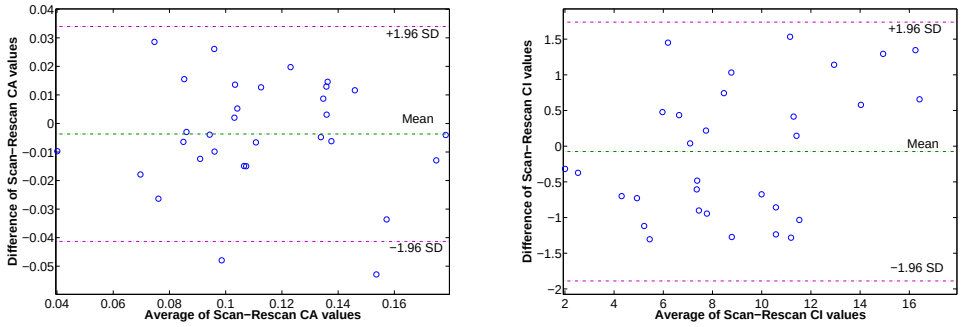

Figure 5.2: The Bland-Altman plots of CA and CI showing the agreement between scan-rescan values. SD: standard deviation.

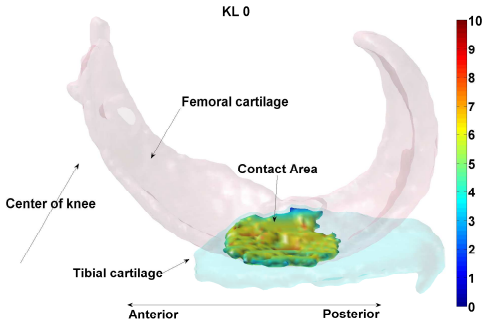

Figure 5.3: Congruity map shown over the CA for a healthy knee used in the cross-validation. Red indicates higher congruity, generally observed in the central regions. Blue indicates lower congruity, generally observed all over the CA and mostly around the periphery. It is plotted at a curvature scale of 2.4 mm and 4 curvature flow iterations.

Table 5.1 for all KL grades. As expected, better reproducibility is achieved for KL 0 subjects than for subjects with higher KL. For the CA, the CV and CC are 13.7% and 0.83 ($p < 0.0001$) respectively. For the CI, they are 7.5% and 0.92 ($p < 0.0001$). The Bland-Altman graphs showing agreement and lack of bias are given in Fig. 5.2 for CA as well as for CI. In general, for all combinations of scale and iterations, the ranges of CV and CC for CA are 13.5% to 13.8% and 0.81 to 0.84 whereas for CI, they are 6.9% to 8.5% and 0.91 to 0.95.

5.4.1 Contact area

The CA is normally located at the anterior part of the tibial sheet and towards the center of the knee. The CA values in general are independent of the parameters. The mean CA for healthy subjects (KL 0) is 0.103. It is significantly increased with onset of OA (KL 1) and is 0.118. The CAs for OA and advanced OA subjects are listed in Table 5.2. The CA significantly separated KL 0 and KL 1 (AUC 0.65, $p < 0.001$). For separating healthy (KL 0) from OA (KL > 0), the CA showed borderline significance with AUC of 0.61 ($p = 0.07$). See Table 5.5 for details.

The CA showed sensitivity to change through reasonable SRMs for all KL grades as shown in Table 5.3. The SRM of Healthy (KL 0) is -0.35 and

increased to -1.14 at advanced stages of the disease.

Table 5.2: Contact Area and Congruity Indices mean and SD values for KL 0, KL 1, KL 2, KL 3/4 subjects respectively at baseline. Fixed parameters were used (2.4mm curvature scale and 4 curvature flow iterations). N: number of knees

KL Index (N)	CA (mean ±SD)	CI (mean ±SD)
0 (145)	0.103 ±0.029	9.6 ±1.5
1 (89)	0.118 ±0.032	8.2 ±1.4
2 (30)	0.106 ±0.040	6.5 ±1.5
3/4 (24)	0.091 ±0.041	4.9 ±2.6

5.4.2 Congruity index

The congruity values decreased with increasing curvature scale due to low curvatures at higher scales. The mean CI for healthy subjects (KL 0) is 9.6. The CI values are lower in early OA and lowered further at later stages of OA (Fig. 5.5). See Table 5.2 for congruity values at healthy and progressed stages of OA. The congruity map for an example healthy knee used in the evaluation is shown in Fig. 5.3. Comparing to CA, the CI also showed ability to separate KL 0 and KL 1 (AUC 0.64, $p < 0.01$). The AUC is 0.69 ($p < 0.0001$) for separating KL 0 vs. KL > 0, and 0.73 ($p < 0.0001$) for separating KL$\leq$ 1 vs. KL > 1. The cross-sectional separation of healthy and different KL knees is shown in Fig. 5.5 for both the CI and the CA.

For the CI, the SRM is good at advanced stages of the OA (-0.21 for KL 3/4). See Table 5.3 for all KL grades.

Table 5.3: The longitudinal SRM of CA and CI for KL 0, KL 1, KL 2, and KL 3/4 knees respectively. Fixed parameters were used (2.4 mm curvature scale and 4 curvature flow iterations). N: number of knees

KL Index (N)	SRM for CA	SRM for CI
0 (126)	-0.35	0.01
1 (78)	-0.47	-0.03
2 (23)	-0.60	-0.04
3/4 (17+1)	-1.14	-0.21

5.4.3 Fixing the parameters

From Table 5.5, if we fix the parameters at a scale of 2.4 mm and 4 iterations for all the diagnostic tasks, there is no significant change in the results presented. The best AUC to separate KL 0 and KL 1 in case of CI occurred at scale 5.4 mm. However, the AUC is still significant at 2.4 mm and 4 iterations (0.62, $p < 0.01$). In case of CA, the best separation of KL 0 and KL 1 is also achieved at the scale of 2.4 mm. The AUC for the other tasks is not significant at any of the proposed scales.

5.4.4 Comparison with a related method

We compared our method with the method described in [4]/[47] for cross-sectional separation of the tasks listed in Table 5.4 at baseline. Our method performs well at separating early stages of OA from healthy, whereas the already existing method is able to separate OA knees from advanced stages of OA. The complete comparison results are listed in Table 5.4 along with the p-values from a DeLong-DeLong test. A scatter plot between our proposed CI and the CI in [13]/[14] is shown in Fig. 5.4 based on the baseline values, the CC is 0.41 ($p < 0.0001$).

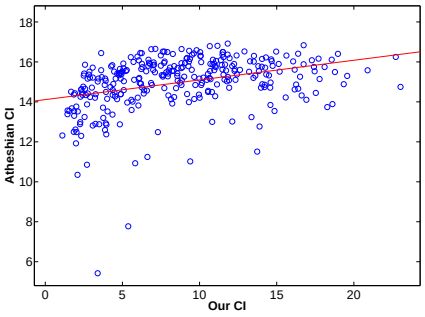

Figure 5.4: The scatter plot between our CI and the CI in [4]/[47] based on the baseline knees including all KL. The red line is the best fit.

Table 5.4: Comparison of our proposed method with the method in [4]/[47] for cross-sectional separation tasks using CI at baseline. Fixed parameters were used (2.4mm curvature scale and 4 curvature flow iterations). The Significance of Difference between the AUC values in the 2nd and 3rd columns is also measured using [22], denoted as P_S. *P < 0.05, **P < 0.01, ***P < 0.001, ****P < 0.0001.

Task	Our proposed CI	Ateshian/Hohe CI	P_S
KL 0 & KL 1	0.62**	0.52	$9e^{-4}$
KL 0 & KL > 0	0.69****	0.58*	0.04
KL ≤ 1 & KL > 1	0.73****	0.74****	0.20
KL 2 & KL 3/4	0.63	0.79****	0.01

Table 5.5: Statistical scores to show the ability of the CA (top rows) and the CI (bottom rows) to separate different groups cross-sectionally at baseline. *p < 0.05, **p < 0.01, ***p < 0.001, ****p < 0.0001. SD: standard deviation.

Measure	Task	Iteration (median ±SD)	Scale (median ±SD)	Training AUC	Validated AUC	RMS CV	CC
CA	KL 0 & KL 1	2 ±6	2.4 ±1.5	0.65**	0.65**	13.7%	0.83****
	KL 0 & KL > 0	4 ±5	5.4 ±1.6	0.62*	0.61	13.5%	0.84****
	KL ≤ 1 & KL > 1	16 ±3	5.4 ±1.3	0.56	0.53	13.5%	0.84****
	KL 2 & KL 3/4	16 ±2	3.4 ±1.5	0.60	0.59	13.6%	0.83****
CI	KL 0 & KL 1	2 ±3	5.4 ±1.0	0.66**	0.64**	7.0%	0.95****
	KL 0 & KL > 0	2 ±2	2.4 ±0.3	0.70****	0.69****	7.9%	0.91****
	KL ≤ 1 & KL > 1	4 ±3	2.4 ±0.4	0.75****	0.73****	7.5%	0.92****
	KL 2 & KL 3/4	8 ±5	2.4 ±1.4	0.73*	0.63	7.2%	0.94****

5.5 Discussion

We developed fully automatic methods for quantification of medial tibiofemoral joint CA and CI. From Fig. 5.3, the contact area is generally located in the anterior load-bearing part of the tibial plateau, which could be due to semi-flexed position of the subject knee in the scanner. In particular, the peripheral part of the cartilage sheet does not contribute to the CA since this region is consistent with the typical location of the meniscus in a healthy joint. The variations of CA (observed in Fig. 5.5) from healthy to early OA might be due to early biomechanical adaptation initiated within the knee. The significant increase in CA values in early OA could be due to meniscal subluxation or tibial/femoral bone flattening or loss of cartilage thickness or combinations of both. The reduction of the CA in advanced stages of OA could be due to loss of cartilage. Since the radiographs for grading OA are acquired in a loaded condition, loaded MRI may potentially be lead to

CA estimation with better diagnostic value than the non-loaded MRI. Such scanners are becoming more widespread and would be interesting to use in a future study. The non-normalized CA values are close to the literature values that were computed non-invasively using MRI [48, 80]. Since we limited ourselves to the medial compartment in this study; comparison to the lateral compartment CA is not possible. The cartilage-meniscus interface/region is ignored in this study since inclusion of the meniscus makes the quantifications cumbersome and we therefore leave it for future studies.

The RMS CV of 13.7% for the CA makes it promising to use as a biomarker; though it is quantified from the non-uniform shapes. The precision is better compared to the mean CV of 15.1% in a previous MRI-based study [48], moreover our scan-rescanned knees constitute healthy and all levels of OA. In a casting study [42], it was shown that, the CAs increased with OA severity and in an invasive study they estimate the CA including meniscus under load [67]. These studies are, however, not directly comparable to our study since we ignored the cartilage-meniscus interface and no load was applied while acquiring the MRI. The precision of the CA estimation may also be improved by using a high field scanner.

The CV of the CI quantification is equal to or better to the CV of an already published CI quantification method [49]. However, it is difficult

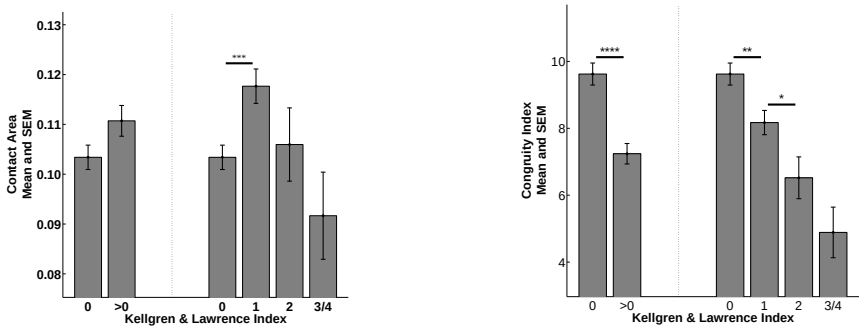

Figure 5.5: Cross-sectional separation of healthy and different KL using the CA and the CI at baseline for the fixed parameters (2.4 mm curvature scale, 4 curvature flow iterations). *P < 0.05, **P < 0.01, ***P < 0.001, ****P < 0.0001.

to compare since our congruity quantification is a local measure and is limited to the CA (which may indeed be the most interesting region) and also different methods were used to locate and segment the cartilage. We employed the mean curvature flow in a level set formulation since it was demonstrated to be a better choice in terms of accuracy at computing the curvatures limited by scan resolution [41]. The precision of the CA quantification might be improved from a shape-model and also expect the similar CA values computed from the shape-model. Similarly, the shape model could compute the curvatures at coarse scales better [41] and thereby benifit the precision of CIs. We may investigate the quantifications using the tibio-femoral shape model in the future.

There is no significant change in the results listed in Table 5.5 using the fixed parameters. Therefore, we affirm that the curvature scale and number of iterations have no significant impact on the diagnosis tasks. Comparing our CI with the alternative CI in [4]/[47], the low correlation and the scores in Table 5.4 shows that it may a good idea to combine first and second order features for better separation of healthy from early OA.

In general, it might be interesting to consider only the CA, the 0^{th} order information to define the congruity in a crude manner. Then, we could say that the larger the CA, the better the congruity. This is more likely true when computing across the entire compartment including the meniscus. In particular, if we assume that the medial compartment is embedded in a Euclidean space, it is incongruent because of the shape of the tibial plateau (flat) and femoral cartilage (C-shaped). However, from the CA cross-sectional separation (Fig. 5.5), we may trust that the meniscus helps in spreading the CA in the compartment, which was also well documented in the literature [42, 53]. We believe that 0^{th} order makes much sense in coarse scale congruity. From the cross-sectional separation (Fig. 5.5), we could say that the inclusion of the cartilage-meniscus region may be vital in quantifying the total CA and CI in the knee. Therefore, the CA excluding the meniscus is not enough to define the CI. Since it is difficult to quantify in the cartilage-meniscus interface, we believe that quantification of the first and second order feature combinations over the CA may provide some insight into the local congruity. If the surfaces are locally conforming, the distance will be close to zero, because of the outward normal vectors scaled

by local signed normal curvature.

5.5.1 Limitations

The congruity measure is dependent on the parameters used to compute the local normal curvatures. This is because at higher scales, the curvature values are lower, resulting in low congruity values. At lower scales the higher incongruities found in the edges of the contact region whereas at higher scales, the incongruities shift to the central regions of the CA. This may be due to that at higher scales, the edges towards the center of the knee become smoother and have less curvature. Nevertheless, the cross-validation estimated the best scale and the iteration number for a specific task and good generalization is achieved (Table 5.5). Currently, the quantifications are applicable to the scans that have nearly isotropic voxels. The moderate inter-scan precision of the CA may be due to that it is quantified from a difficult geometrical shape and also that it varies with flexion angle. However, it was attempted to position the knee at the similar flexion angle during baseline and follow-up visits. Nevertheless, we would like to measure and optimize the knee angle in future studies for making the measurements more robust.

The local congruity quantification is sensitive to local curvature in the CA. However, with an RMS CV of 13.7% we feel that, it is fair to conclude that we have investigated small knee angle changes. Further, the sensitivity of the CA and CI to large angle changes needs to be studied. Since we are contrasting between healthy and OA individuals, the near full extension in supine position may be the most comfortable position while acquiring the scans. Nevertheless, it is pertaining to see the ability of the presented method validated on the scans acquired at various flexion angles. Finally, the load is modelled as a step function, however, in future studies, nonuniform load distributions could be considered.

In this work, we focused on the diagnostic capabilities of the CA and CI. Another potential of the biomarker, however, lies in its ability to predict disease progression. The current study population had good SRMs and also showed borderline ability ($p < 0.05$) to predict radiographic OA and to predict the MTF cartilage volume loss for select KL grades only. Specifically, in experiments not included above, borderline significance

was achieved for predicting longitudinal cartilage loss for KL 1 ($p < 0.05$) and predicting JSN for KL 3 ($p < 0.05$). However, as it is difficult to conclude based on sub-population scores, future studies on large populations are needed to generalize the ability of the presented quantifications as a marker for predicting the disease.

5.6 Conclusions

The MTF joint CA and CI are quantified non-invasively, and are capable of contrasting healthy from OA subjects. The CA quantifications might be used to separate healthy and early OA knees with an AUC of 0.65 ($p = 0.004$). The congruity is generally highest in healthy knees and decreases with onset of OA and further with disease severity (AUC to separate KL 0 & KL > 0 is 0.69, $p < 0.0001$). The decrease in the CA and the CI over 21-month period at advanced stages of OA may be due to changes in bone flatness, and apparent decrease in local congruency respectively. The proposed methodology could be applied to other knee compartments and maybe to other load-bearing joints. Future quantifications could include the meniscus to compute the overall CA and CI to elucidate their changes with OA progression. In conclusion, the quantification methods might be suitable to help explaining the onset, diagnosing (early) OA, and measuring the efficacy of DMOADs in clinical trials.

Chapter 6

Gender differences in contact area and congruity index are explored. Main results are in Figure 6.1 and Table 6.2, 6.3, 6.4.

Gender differences in Tibio-Femoral Contact Area and Congruity Index from MRI

Tummala S, Schiphof D, Byrjalsen I, Dam EB
This chapter is based on the manuscript that is submitted to Osteoarthritis and Cartilage

Objective: The aim of the study was to investigate gender differences in the medial tibio-femoral (MTF) compartment contact area and congruity quantified automatically from magnetic resonance imaging (MRI).
Methods: At baseline (BL), 81 male and 78 female community-based subjects aged 21 to 81 with normal or OA-affected knees were recruited. The

MRI and radiographs were acquired for all subjects at both visits. The MTF compartment was segmented fully automatically using a voxel classification approach. From the MTF, the Contact Area (CA) was quantified using Euclidean distance transform by employing the voxel width as threshold. Further, the Congruity Index (CI) was quantified over CA by assessing the first and second order general surface features. Gender differences between CA and CI were evaluated along with their ability to separate healthy and OA knees, sensitivity to change, correlations with changes in MTF cartilage volume, and JSW.
Results: The 21-month longitudinal study was concluded by 72 male and 68 female subjects. At BL, male CA were significantly lower than female CA ($p \approx 10^{-8}$ for healthy) and male joints were more congruent than female joints ($p \approx 10^{-11}$ for healthy). The differences were significant after adjusted for age and BMI. The CA demonstrated sensitivity to change at all stages of KL (e.g. SRM of -0.73 and -0.91 for male and female joints). Correlations between cartilage volume change and CI changes were stronger in females.
Conclusions: This study demonstrated that there existed gender differences in CA and CI in MTF joint. The lower CI values in female knees may be associated with risk of female gender for Osteoarthritis. These differences may help to further understand the gender differences and/or to establish better treatment strategies for females.

6.1 Introduction

Osteoarthritis (OA) is a major health concern worldwide causing pain and limited range of motion in major load bearing joints in elderly [15]. There are several systemic and non-systemic risk factors that contribute towards the development and progression of the OA [38]. Gender is one of the systemic risk factors in the onset of OA [13, 90]. There are several factors that contribute to the predisposition of OA in women. Some of the factors could be cartilage structure, hormonal imbalance, biomechanics, malalignment, age and exercise. Biomechanical factors in general play a significant role in the onset of OA [54] and previous research showed there existed gender differences in the biomechanics of the OA knees [72]. Age play a

critical role to make women susceptible to OA significantly more than men generally from the onset of menopause [17].

Studies assessed the gender differences from the longitudinal volume change, gait analysis, pain and correlation of clinical OA with Kellgren & Lawrence (KL) score [45] Starting with non-invasive studies from cadavers, the gender differences in patello-femoral joint biomechanics were explored [24] and concluded that women had less contact areas and greater contact pressures in the patella-femoral joint. In [5], the gender differences in thumb carpometacarpal (CMC) joints Congruity Index (CI) were explored and concluded that male joints were more congruent than female joints; also concluded that the lower congruity may be the risk factor for development of CMC joint OA in females.

MRI has become a major imaging modality in OA research since it allows non-invasive visualization of all the tissues present within the joint especially the cartilage [43]. In [9, 21, 31], knee cartilage volume and bone mineral density differences were validated and men have significantly more cartilage than women after adjusted for confounding factors age and body mass index (BMI). Women showed smaller joint surfaces and thinner cartilage as compared to men after adjusting for height and weight [**?**, 77]; however, there were no differences in tibial and patellar surface pressures. The gender differences in morphometric measurements from radiographs, MRI and biochemical markers were detailed in [71, 75] and suggested the needs for future research to explore on implications for gender based treatment options.

The contact area (CA) in the MTF joint is the region, where the articular cartilage surfaces that cover the ends of the bones are in close proximity. In the CA, the two surfaces interact and transfer the local stresses, and thereby causing no or insignificant degeneration to the cartilage in a healthy joint. We refer to the CA as the cartilage-cartilage contact area but not the cartilage-meniscus contact area. The 'Congruity' could physically be defined as how well any two surfaces fit together. In a healthy tibiofemoral joint, the smooth femoral cartilage surface articulates well with the tibial cartilage surface and is congruent in association with the meniscus.

In this study, we investigated the following on a study population, stratified according to KL index. a) The gender differences in the medial tibio-

femoral joint CA and CI quantified automatically. b) The gender differences in the sensitivity to change in the CA and CI over 21 months. c) The gender differences in the associations of longitudinal percentage change in CA and CI with the longitudinal percentage changes in tibio-femoral cartilage volume and with joint space width (JSW).

6.2 Methods

The method section includes X-ray and MRI protocols used for image acquisition. Computation of MTF cartilage volume, joint space width (JSW), and pain are briefly described. Quantification methods for CA and CI, statistical methods used for validation are also described.

6.2.1 Study Population

The study population consisted of 82 male and 77 female subjects selected from the greater Copenhagen. The population consists of subjects with age range 21-81 and with varying degrees of radiographic OA. Subjects with a history of previous knee injury or trauma; or contradiction to image acquisition were excluded from the study. The range of the interval between baseline and follow-up visit was 15 to 21 months with an average of 18 months. At baseline (BL), we also have manual tibial and femoral cartilage segmentations for 59 male and 55 female subjects from the same population to compare with automatic segmentations. More details on the study population is described elsewhere [26].

6.2.2 Image Acquisition

We have 318 knees at BL. Five out of 318 knees were excluded due to insufficient image quality in either MRI or X-ray. Another 25 knees used for training of classifier for automatic cartilage segmentation were excluded from the evaluation. Both the knees of each subject were scanned using X-ray and MRI. The radiographs were scanned in anterior-posterior load bearing position. The radiographs were used to grade the severity of OA using the Kellgren & Lawrence Index (KL) and also to measure the joint

space width (JSW) by an experienced radiologist [60]. The MRI scans were acquired in a non-load bearing supine position using a Turbo 3D T1 sequence at 0.18T from an Esaote C-span scanner dedicated to scan the extremities of the body. The parameters of the scanner were 40^0 flip angle, 50 ms repetition time and 16 ms echo time with scan time of approximately 10 min. The in-plane resolution was 0.7 mm x 0.7 mm with slice thickness ranging from 0.7 mm to 0.9 mm.

6.2.3 Cartilage Volume and Joint Space Width Quantification

In this study, we quantified the medial compartment, since knee OA most often is observed in the medial side [29, 66]. The MTF cartilage compartments were segmented fully automatically using a voxel classification approach [41]. The volume of the compartment was measured in mm^3 by counting the voxels and then multiplying by the scan resolution. The volume values were normalized to the tibial bone width (TBW) excluding osteophytes to avoid the bias between knee size variation due to age, sex and other growth factors. The volume was multiplied with the cubed ratio of mean TBW to the TBW of the respective knee. The joint space width (JSW) was measured in mm as the narrowest gap between femur and tibia within the medial tibial plateau.

6.2.4 Contact Area and Congruity Index Quantification

The contact area in a knee was defined as the region where the tibial superior surface and the femoral inferior surface were less than a voxel width apart. It was estimated using the Euclidean distance transform. Firstly, the tibial surface that was less than a voxel width from femoral surface was estimated and called *TibProx*. Secondly, the femoral surface that was less than a voxel width from the tibial surface was computed and denoted as *FemProx*. The solid areas of *TibProx* and *FemProx* were quantified by converting the estimated region into a triangulated surface. The CA eventually was the mean of the area of *TibProx* and the area of

FemProx since the cartilage surfaces were not symmetric.

$$CA = \frac{A_{TibProx} + A_{FemProx}}{2} \tag{6.1}$$

The CA values were also normalized using TBW. The CA of each knee was then multiplied with squared ratio of mean TBW to the TBW of the corresponding knee. The point-by-point Congruity Index (CI) on the *TibProx* and *FemProx* was quantified by assessing the first and second order general surface features. The final CI of MTF compartment was the mean of the CI quantified from *TibProx* to *FemProx* and vice versa. Let *TibProx* has N_1 points and *FemProx* has N_2 points, mathematically final CI of MTF joint would be as follows:

$$CI = \frac{\frac{\sum_{p=1}^{N_1} CI_p}{N_1} + \frac{\sum_{q=1}^{N_2} CI_q}{N_2}}{2} \tag{6.2}$$

CI_p and CI_q are CIs at the points p and q respectively. The MTF joint was said to be locally congruent if the distance between the local surface normal vectors (first order features) scaled by local surface normal curvatures (second order features) was minimum. For instance, mathematically, the CI_p was detailed below.

$$CI = \frac{1}{||k_t n_t - k_f n_f||} \tag{6.3}$$

where n_t and n_f were the tibial and femoral local normal vectors computed from gradients and gradient magnitudes of level set representation of tibial and femoral cartilage compartments respectively. Further, k_t and k_f were the tibial and femoral local curvatures computed along the direction of major knee motion (flexion/extension) using Euler's formula. See Figure 6.1 to visualize the location of the contact area and local congruity index map for a knee used in this study.

The methodology is explained in Chapter 5. Please see it for complete technical details of CA and CI quantification.

6.2.5 Statistical Analysis

Whether any two groups of measures were different was evaluated using p-value (P) from Student's T-test. The association between any two groups was calculated using Pearson's linear correlation coefficient (CC). The longitudinal responsiveness was quantified as Standardized Response Mean (SRM) which was the ratio of mean change to the standard deviation of change between follow-up and baseline visit. The effect of potential confounding factors age and BMI were applied using a linear correction if there were any significant correlations with the measure (CA and CI). The statistics were performed using MATLAB R2011b (Mathworks Inc). A 0.05 level was used throughout the paper for statistical significance.

6.3 Results

The longitudinal study was concluded by 72 male and 67 female subjects. The age and BMI of the population were evenly distributed at BL as well as at FU according to gender and further arranged with respect to KL index (Table 6.1).

Table 6.1: Table showing the number of knees (N), Age (in years) and BMI (kg/m^2) for male and female subjects used in the evaluation at Baseline (288) and at follow-up (245) with respect to KL index. Stars indicate the significance of difference between the genders for Age and BMI for that specific KL index. The significance of difference between genders was added to the female demographic. *p < 0.05, **p < 0.01, ***p < 0.001, ****p < 0.0001.

	Baseline						Follow-up					
	Male			Female			Male			Female		
	N (knees)	Age (mean)	BMI (mean)	N (knees)	Age (mean)	BMI (mean)	N (knees)	Age (mean)	BMI (mean)	N (knees)	Age (mean)	BMI (mean)
All KL	148	23-77 (57)	20-38 (27)	140	21-81 (56)	18-37 (26)*	127	25-79 (56)	20-36 (27)	118	23-83 (58)	18-36 (25)***
KL 0	79	23-77 (49)	20-38 (25)	66	21-78 (47)	18-36 (24)*	53	25-75 (50)	20-34 (25)	48	23-80 (47)	18-35 (23)**
KL 1	40	46-77 (64)	20-34 (27)	48	37-81 (61)	19-37 (26)*	49	29-79 (64)	21-36 (28)	47	36-83 (63)	20-36 (26)**
KL 2	16	56-70 (65)	24-37 (31)	15	47-78 (67)	22-34 (28)*	12	59-74 (67)	21-31 (28)	14	49-80 (68)	22-36 (28)**
KL 3/4	13	61-72 (68)	23-34 (29)	11	58-78 (67)	23-34 (28)	13	62-73 (69)	24-35 (29)	9	59-80 (68)	22-32 (28)

6.3.1 Cross-sectional separation of CA at Baseline and at follow-up

The location of the CA in a MTF joint is shown in Figure 5.4. The CA was located in central load-bearing regions of the compartment.
Stratification of CA according to KL index for the male and female subjects at baseline was shown in Figure 6.1. The CAs for male subjects were not significantly different with respect to KL index whereas for female joints, the CAs were significantly different between healthy and early OA (KL 1) subjects ($p < 0.05$). In general the CAs of the female subjects were larger than the male subjects from healthy to all stages of OA (Table 6.2).
The same pattern of separation was found at follow-up.
There was no significant correlation between CA and age, CA and BMI for male. In case of female there was a significant correlation (CC = 0.20, $p < 0.05$) between CA and age, between CA and BMI (CC = 0.40, $p < 0.001$).

Table 6.2: The table shows CA and CI values of Male and Female at Baseline as well as at Follow-up. The significance of difference between genders computed as p-value from t-test was added to the female values. M: Male, F: Female, CA: Contact Area, CI: Congruity Index. *p < 0.05, **p < 0.01, ***p < 0.001, ****p < 0.0001.

	Baseline				Follow-up			
	CA Male	CA Female	CI Male	CI Female	CA Male	CA Female	CI Male	CI Female
Healthy (KL 0)	552 ±138	703 ±178****	12.0 ±4.1	7.1 ±4.3****	474 ±161	651 ±163****	12.2 ±4.1	7.9 ±4.1****
Early OA (KL 1)	598 ±160	791 ±175****	9.3 ±4.6	6.9 ±3.5****	525 ±177	692 ±198****	9.7 ±3.5	7.1 ±3.7****
OA (KL > 1)	519 ±234	678 ±232**	6.3 ±3.7	5.3 ±3.9****	393 ±218	567 ±208***	6.8 ±3.9	6.0 ±3.8

6.3.2 Cross-sectional separation of CI at Baseline and at follow-up

The similar trends were observed for cross-sectional separation of CI according to KL index for both male and female at baseline as well as at follow-up (see Figure 6.2 for baseline). The CIs for male joints were significantly different between KL 0 and KL 1 ($p < 0.0001$) at BL as well as at

FU. In general, healthy male joints were more congruent than male joints with OA ($p < 0.0001$). The CIs of the female joints were generally lower and not different between healthy and OA ($p = 0.40$). See Figure 6.2 for comparison of mean CIs for male and female subjects with respect to KL index. In general, the male joints were more congruent than female joints at healthy and early OA ($p < 0.0001$) but not at advanced OA ($p = 0.33$, see Table 6.2 for complete details).
There was no significant correlation between CI and age, CI and BMI for male. In case of female there was a significant correlation (CC = -0.39, $p < 0.001$) between CI and age, no correlation between CI and BMI.

6.3.3 Responsiveness of CA and CI

The longitudinal SRMs were higher for both genders in case of CA at all stages of KL index (Table 6.3). For instance, the SRM for CA at advanced stages of OA was -0.73 and -0.91 for male and female joints respectively. The SRM for CI was not different between genders and generally higher at healthy compared to advanced OA.

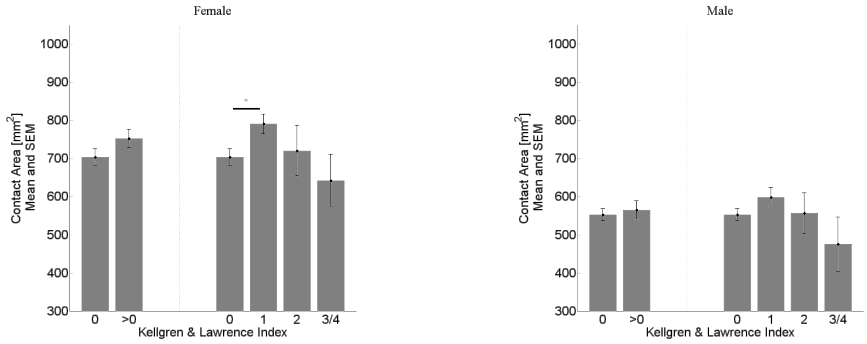

6.3.4 Efficacy of CA and CI

There existed strong correlations with longitudinal percentage change in MTF cartilage volume with longitudinal percentage change in CA as well as with CI for both genders (Table 6.4). Correlations were in general stronger in female subjects in case of CI. For example, the correlation between cartilage volume changes and CI changes for advanced OA female joints

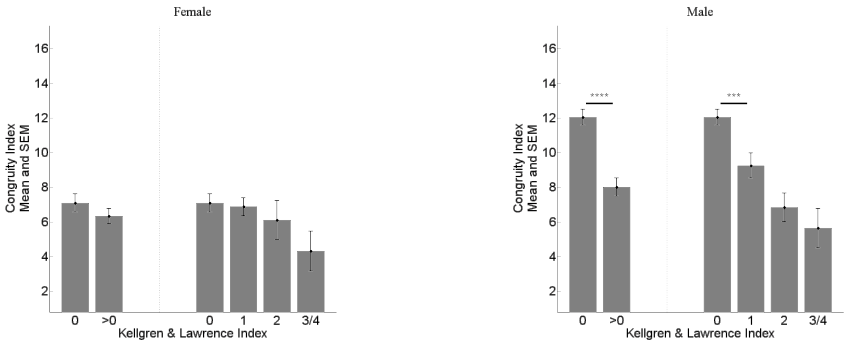

Figure 6.1: Cross-sectional separation of healthy and different KL for male and female subjects based on Contact Area and Congruity Index at baseline. Contact Areas were higher for female after adjusted for tibial bone width. Congruity indices were smaller for female knees. The stars indicate the statistical significance computed from Students t-test. *P < 0.05, **P < 0.01, ***P < 0.001, ****P < 0.0001.

was 0.87 ($p < 0.0001$) and it was 0.14 for male subjects. Further, significant correlations existed between JSN and longitudinal changes in CA for early OA (0.39, $p < 0.05$) male joints. See Table 6.4 for correlations with female joints.

Table 6.3: The sensitivity to change over 21 months for CA and CI for Male and Female subjects for Healthy (KL 0), early OA (KL 1), and OA (KL > 1) were listed. SRM: Standardized response mean, CA: Contact Area, CI: Congruity Index.

	SRM Male		SRM Female	
	CA	CI	CA	CI
Healthy (KL 0)	-0.46	-0.10	-0.22	0.29
Early OA (KL 1)	-0.41	-0.02	-0.52	-0.05
OA (KL > 1)	-0.73	-0.03	-0.91	-0.11

6.4 Discussion

We explored the gender differences in medial tibio-femoral CA and CI along with their ability to separate healthy and OA subjects, with their ability to detect longitudinal changes, efficacies, and relation with pain. The results corroborated that there may be gender differences in the onset of OA from a biomechanical points of view. For healthy biomechanics of

synovial joints, there are different tissues (cartilage, meniscus) involved in transmitting the load effectively during all daily activities. The significant increase in cartilage-cartilage CA from healthy to early OA in female joints suggests that the meniscus likely play a role in the onset of biomechanical instability in the joint. The higher CAs of the female subjects after adjusting for bone width suggests that more cartilage area may be involved in load transmission than compared to male joints. The lower CA values at advanced stages of OA were may be due to loss of cartilage. Malalignment (Q-angle) may be responsible for local congruency in the joint. However, it was hypothesized that local incongruity plays a role in determining the alignment [52]. Therefore, since male healthy joints were more locally congruent, this may be responsible for lower malalignment in males compared to females.

We evaluated and observed the similar trend of cross-sectional separation for CA and CI at BL as well as at FU to affirm the differences. One may speculate whether the existed differences in CI were due to algorithmic artifacts. Therefore, we computed the CI on manual segmentations and demonstrated a p-value of $6e^{-6}$ to separate male and female; it supports that the observed differences were due to differences in congruity indices and not due to algorithmic artifacts. Female joints CIs were significantly lower than the male joints CIs irrespective of source of segmentations.

The CA demonstrated good SRM for both genders. The SRMs shows that the cartilage-cartilage contact area was reduced at follow-up which may be due to several phenomenon including meniscal extrusion, bone flattening and combinations of them. However, the SRMs for CI were lower compared to CA for both genders.

There existed strong correlations between longitudinal change in tibiofemoral volume and with longitudinal change in CA and CI. Particularly, the correlations between volume change and CI changes were stronger in females at early and advanced stages of OA. Therefore, local congruity may be one of the early denominators in OA, especially in females. There were borderline significant correlations between JSN and CA and CI changes also supporting that. The lower congruity values in females may be associated to the biochemical protein IGF-1 which is responsible for strength of the muscles [95]. The muscle strength may also be an important factor

Table 6.4: Correlations of CA and CI longitudinal percentage changes with tibio-femoral cartilage volume percentage change, JSW percentage change for male and female subjects listed for Healthy (KL 0), early OA (KL 1) and OA (KL > 1) subjects. CA: Contact Area. CI: Congruity Index. M: Male, F: Female, MTF: medial tibio-femoral, JSW: joint space width. *p < 0.05, **p < 0.01, ***p < 0.001, ****p < 0.0001.

	MTF cartilage % change				JSW % change			
	CA % change (M)	CA % change (F)	CI % change (M)	CI % change (F)	CA % change (M)	CA % change (F)	CI % change (M)	CI % change (F)
Healthy (KL 0)	0.20	0.42**	0.44***	0.35**	0.11	0.19	0.22	0.01
Early OA (KL 1)	0.37*	0.73****	0.44**	0.75****	0.39*	-0.07	0.21	0.10
OA (KL > 1)	0.53*	0.41*	0.14	0.87****	0.31	0.28	-0.10	-0.08

in making the joint less lax and more congruent and stable.

The performance of CA and CI for cross-sectional separation of healthy and OA for male was confounded with neither age nor BMI. Therefore, the measures performances as diagnostic marker were retained. On the other hand, interestingly, females those have older and higher BMI have more CA which may be possible. Young females were also more congruent than older females. The cross-sectional separation of healthy and OA based on CA and CI for female after adjusting for age and BMI does not change significantly.

There were some limitations in this study. A low-field scanner was used in this study. The main disadvantages of low-field scanners are lower signal-to-noise ratio and spatial-temporal resolution. A low-field scanner has the advantages of low cost for installation, scanning and maintenance. Nevertheless, the results need to be reproduced on high-field scanners. Since the measures contact area and congruity index depend on the knee angle, we were not able to validate the current gender differences on other flexion angles. We were also not able to optimize the knee angle at which the maximum gender differences could be extracted. However, for consistency with healthy and advanced OA knees, we feel that the non-load-bearing supine position was a good position. The study population was also somewhat small to validate the effect of menopause thoroughly which occurs around the age of 50. We want to evaluate this on a large study population.

In conclusion, we conducted a study to explore the gender differences in MTF joint contact area and congruity from MRI. Significant gender differences were found in contact area and congruity at healthy and early stages of OA. The existing differences may be helpful to understand the Gender differences in healthy subjects and those with knee OA and further may provide implications for making gender specific treatment strategies. Future studies on large populations and from different scanners are needed to confirm the findings.

Chapter 7

Summary and General Discussion

Imaging modalities provide non-invasive input for sophisticated research in OA for the discovery and characterization of novel biomarkers. The KL index and JSW from radiographs still is the gold standard marker and the novel markers from MRI would help to understand the early disease changes. The measures (CSS, CA, CI) that were related to cartilage quality and biomechanics showed ability to separate healthy and diseased. In general, CA and CI were able to separate healthy (KL 0) from early ROA (KL 1). These methods could be applied to other knee compartments as well as other joints in the body.

7.1 Summary

In Chapter 2, we presented the CSS quantification method in the MTF cartilage compartment. The ability to seperate healthy and OA is com-

pared between manual and automatic segmentations. In Chapter 3 and 4, smoothness markers measured in the tibial and central femoral compartments, which are also the most load-bearing compartments, were the most reliable indicators of the presence of OA. This supports an intuitively reasonable relationship between biomechanical stress and loss of cartilage surface smoothness. The smoothness markers performed better to separate KL ≤ 1 & KL > 1 than KL 0 from KL > 0 (Chapter 3). The CA quantifications might be suitable to separate healthy and early OA. The congruity was generally highest in healthy knees and decreases with onset of OA and further with disease severity. The CSS methodology and the proposed CA and CI quantification methodologies could be also applied to other knee compartments and maybe to other load bearing joints in the body. The CI quantification method in Chapter 5 is novel and showed ability to separate KL 0 from KL > 0 in general (AUC 0.69, $p < 0.0001$). Significant gender differences were found in contact area and congruity index at healthy and early stages of OA. In Chapter 6, we demonstrated these differences that may be helpful to understand the Gender differences and further to provide implications for making gender specific treatment strategies. Future validation studies on large populations and from different scanners are needed to confirm the abilities of CSS, CA and CI as appropriate biomarkers of OA. The fully automatic markers performed better than the markers based on manual segmentations and better than the alternative markers measuring cartilage volume and JSW for separating healthy and OA. The potential future implications are better and earlier OA diagnosis as well as radiologist relief.

7.2 Markers Precision

The precision of the smoothness markers in all compartments - tibial, femoral, and femoral sub-compartments - was equal to or superior to that of the volume markers. For most compartments, the smoothness RMS CV scores were around 3 % (see Table 4.2). The RMS CV of 13.7 % for CA is good enough to use it as a biomarker; however it is quantified fully automatically with non-uniform shapes. This CV was better compared to the mean CV of 15.1 % in a previous MRI-based study [48], moreover our

scan-rescanned knees constitutes healthy and all levels of OA. The RMS CV of the proposed CI (7.5 %) was equal or better than the CV of the already existed congruity indices [49]. In general, smoothness markers achieved better precision than the CA and CI. It may be due to that the smoothness quantification involves voxel super-sampling and the computed scores become robust. The CI does not perform better with voxel super-sampling and it is also computationally expensive because of the mean curvature flow for both the tibial and femoral compartments.

7.3 Diagnosis of OA from CSS, CA and CI

The smoothness markers also allowed diagnostic separation of healthy and early OA in all compartments with AUC scores between 0.72 and 0.82. These scores were superior to the cartilage volume scores for reliably diagnosing OA by KL score (e.g. the AUC for femoral smoothness of 0.80 was higher than 0.57 for volume, $p < 0.0001$). A comparison with the diagnostic performance of JSW is less interesting since JSW is a criterion in defining the KL score. As Figure 3.3 illustrates, in addition to the diagnostic separation between healthy knees and those with the higher KL scores, the smoothness markers also allowed separation at later stages of OA. The variations of CA (observed in Figure 5.3) from healthy to early OA might be the due to early biomechanical adaptation initiated within the knee. The significant increase in CA values in early OA could be due to meniscal subluxation or femoral bone flattening or loss of cartilage thickness or combinations of them. The reduction in the CA in advanced stages of OA could be due to loss of cartilage. The CI in general, was able to separate healthy from early OA and in general healthy from OA (Table 5.5).

7.4 Efficacy of CSS, CA and CI

The results in Table 4.4 demonstrated that longitudinal progression in smoothness was related to longitudinal cartilage loss. For instance, the correlation coefficient calculated for yearly change in smoothness versus volume (0.41) in the femoral compartment showed a strong relation ($p <$

0.0001). These strong associations indicate that smoothness markers may be appropriate not only to measure cartilage quality at a given point of time, but may also be useful indicators of longitudinal disease progression, and thus could potentially become markers of efficacy in clinical studies of OA.
There existed strong correlations between longitudinal change in tibiofemoral volume and with longitudinal change in CA and CI. Particularly, the correlations between volume change and CI changes were stronger in females at early and advanced stages of OA. Therefore, local congruity may be one of the early denominators in OA, especially in females. There were borderline significant correlations between JSN and CA and CI changes also supporting that. However, the correlations with JSN were not significant for smoothness as well as for CA and CI.

7.5 Prognosis of MTF cartilage loss and JSN

In the current cohort, the CSS does not show any statistical significance to predict either MTF cartilage loss or JSN for both tibial and femoral compartments. The CSS of femoral central compartment showed borderline ability to predict the cartilage loss ($p = 0.041$). The non-linear progression of the disease may makes it difficult for a marker to predict the loss. The CA and CI showed ability to predict volume loss and JSN in some sub-populations. For example, CI showed ability to predcit cartilage loss for KL 1 subjects only. It involves the measurements at four times which makes the analysis cubersome. The real challange for any marker lies in predicting the JSN, which is the current gold standard. It would be more fruitful to investigate the potential for prognosis in larger populations where it is possible to stratify into different sub-populations that may be more homogeneous (and thus more appropriate for predicting anything from).

7.6 Related Works & Improvements

Large scale curvature analyses were performed both by Hohe et al [49] and Terukina et al [96] on the cartilage surface shown by MRI. However,

these large scale measurements were related to joint congruity rather than smoothness. Efforts have been made to evaluate surface roughness from ultrasound by Chiang et al [20] and most recently by Kaleva et al [55]. The surface roughness index was estimated acoustically for diagnosis of early OA. Ateshian et al [5] used stereophotogrammetry to collect data from human thumb carpometacarpal joints, and curvature maps were calculated by taking the inverse of the osculating circle fitted at every surface point. However, due to the invasiveness, these methods are not feasible for clinical studies. Our CI performed better than the alternative CI by Ateshian/Hohe for early OA. It also shows that it may a good idea to combine first and second order features for better separation of KL at early stages of the OA. The Ateshian/Hohe CI performed better separating KL 2 and above. The CSS, CA and CI markers used in the current study relies on fully automated quantification from non-invasive low-field MRI.
Previously, the accuracy of the fine scale curvature quantification method was validated using digital phantoms [39]. Here, the evaluation for comparing the quantifications based on manual and automatic segmentations was performed to investigate this. The fundamentally different nature of slice-wise 2D manual outlining and 3D automatic segmentation creates fundamentally different segmentation artifacts. The fact that similar results were obtained based on these two segmentation sources indicate that the quantifications are indeed given by the cartilage surface/congruity rather than segmentation artifacts.

7.7 Limitations

The non-invasiveness of the MRI-based smoothness quantification complicates a physical validation of the estimated surface curvatures. In the present study, a physical validation of cartilage quality, for instance, by histology, would have been not feasible in such a large general population of subjects. In addition, low-field MRI has been validated less than high-field MRI for cartilage morphometry. The main limitations of low-field MRI are a lower signal-to-noise ratio and a lower spatial-temporal resolution compared with high-field MRI. However, low-field MRI has advantages of low costs for installation, scanning and maintenance, and in some settings,

low-field MRI has the potential to reduce overall cost with little loss of diagnostic performance [46]. This is of interest for large clinical studies.
Moreover, the results need to be reproduced on high-field scanners. Since the measures CA and CI varies with the knee angles, we were not able to validate the current gender differences on other flexion angles. However, for consistency with healthy and advanced OA knees, we feel that the non-load-bearing supine position was a good position.
The moderate inter-scan precision of CA may be due to that it was quantified from the difficult geometrical shape and also it varies with flexion angle. However, the subject was very likely positioned the knee at the similar flexion angle during baseline and follow-up visit.

7.8 Future Prospects

The thesis also opens research into other interesting biomechanical factors such as friction and stability to quantify them non-invasively from MRI. Since synovial fluid play a significant role in lower joint friction, estimation of synovial fluid may not be trivial. Also, a combination marker of all biomechanical variables could be developed for better diagnosis and prognosis. Another could be to measure the variables from a load-bearing MRI. Currently, the quantifications were applicable to the scans that have nearly isotropic voxels. However, a tibio-femoral cartilage shape model may be a good alternative for generalization and may show better precision. The meniscus could be included while computing the overall medial tibio-femoral contact area and congruity index to elucidate the changes with disease progression.
In the knee, coefficient of friction (COF) is low due to lubrication provided by the synovial fluid in a healthy joint. Moreover, the synovial fluid is generally responsible for low COF in the load-bearing regions of the tibio-femoral compartments and thereby ensures better lubrication during daily activities. Therefore, the joint is healthier if the load regulated by the synovial fluid is higher.
The COF due to synovial fluid is lower compared to solid friction due to cartilage surface asperities in the load-bearing regions of the tibial cartilage superior surface and femoral cartilage inferior surface. The density of

cartilage cells in the superficial zone of the articular cartilage are important for solid phase load transmission. In a recent study, the superficial zone proteins correlated with friction coefficients and advanced OA patients showed higher friction coefficients [74]. The coefficient of static friction in animal joint cartilage surfaces was between 0.005 and 0.02 which is generally considered low [19]. As high loads are transmitting through the joint low friction coefficients are of extreme importance for healthy mechanical functioning.
The different methods used in the literature to compute the friction of the articular cartilage was given in [32]. These methods include whole joint in pendulums, cartilage plugs with custom-built apparatuses, and atomic force microscopy. Apart from the methods in [32], frictional properties of the articular cartilage were studied using tribology [73]. Using instrumentation, the COF in the knee was measured invasively by moving the one cartilage on another in an artificial fluid environment and by measuring the COF as the ratio of the frictional/sliding force to the normal force measured using force transducers [87]. In another study, a pendulum apparatus was used to compute COF in guinea pig knees [94]. In Teeple et.al [94], the COF were contrasted between healthy and guinea pig Osteoarthritic knees and the reported COF values were higher in OA knees. It is more interesting to estimate/quantify the friction in the knee non-invasively from MRI.

In conclusion, the cartilage quality and the biomechanics may be the important factors in the early stages of ROA. The healthy cartilage surface was smoother than the diseased cartilage surface. The cartilage-cartilage CA may be an useful indicator to study the meniscal changes in the early stages of ROA. The healthy joint was more locally congruent than the joint with OA. Male joints were locally more congruent than female joints. The ability of the markers to predict cartilage loss/JSN needs to be validated on larger study populations.

Bibliography

[1] Abramson, S. B., Attur, M., Yazici, Y., (2006). Prospects for disease modification in osteoarthritis. Nat Clin Pract.Rheumatol 2, 304-312.

[2] Andriacchi, T. P., Mundermann, A., Smith, R. L., Alexander, E. J., Dyrby, C. O., Koo, S., (2004). A framework for the in vivo pathomechanics of osteoarthritis at the knee. Ann Biomed.Eng 32, 447-457.

[3] A. A. Qazi, E. B. Dam, M. Nielsen, M. A. Karsdal, P. C. Pettersen, and C. Christiansen, "Osteoarthritic cartilage is more homogeneous than healthy cartilage: identification of a superior region of interest colocalized with a major risk factor for osteoarthritis," Acad. Radiol., vol. 14, no. 10, pp. 1209-1220, Oct.2007.

[4] Astley, S. M., Gilbert, F. J., (2004). Computer-aided detection in mammography. Clinical Radiology 59, 390-399.

[5] Ateshian, G. A., Rosenwasser, M. P., Mow, V. C., (1992a). Curvature characteristics and congruence of the thumb carpometacarpal joint: differences between female and male joints. J.Biomech. 25, 591-607.

[6] Bauer, D. C., Hunter, D. J., Abramson, S. B., Attur, M., Corr, M., Felson, D., Heinegard, D., Jordan, J. M., Kepler, T. B., Lane, N. E., Saxne, T., Tyree, B., Kraus, V. B., (2006). Classification of osteoarthritis biomarkers: a proposed approach. Osteoarthritis Cartilage 14, 723-727.

[7] Bay-Jensen, A. C., Hoegh-Madsen, S., Dam, E., Henriksen, K., Sondergaard, B. C., Pastoureau, P., Qvist, P., Karsdal, M. A., (2009).

Which elements are involved in reversible and irreversible cartilage degradation in osteoarthritis? Rheumatol.Int.

[8] Bellamy, N., Buchanan, W. W., Goldsmith, C. H., Campbell, J., Stitt, L. W., (1988). Validation study of WOMAC: a health status instrument for measuring clinically important patient relevant outcomes to antirheumatic drug therapy in patients with osteoarthritis of the hip or knee. J Rheumatol 15, 1833-1840.

[9] Berry, P. A., Wluka, A. E., Davies-Tuck, M. L., Wang, Y., Strauss, B. J., Dixon, J. B., Proietto, J., Jones, G., Cicuttini, F. M., (2011). Sex differences in the relationship between bone mineral density and tibial cartilage volume. Rheumatology (Oxford) 50, 563-568.

[10] Bingham, C. O., III, Buckland-Wright, J. C., Garnero, P., Cohen, S. B., Dougados, M., Adami, S., Clauw, D. J., Spector, T. D., Pelletier, J. P., Raynauld, J. P., Strand, V., Simon, L. S., Meyer, J. M., Cline, G. A., Beary, J. F., (2006). Risedronate decreases biochemical markers of cartilage degradation but does not decrease symptoms or slow radiographic progression in patients with medial compartment osteoarthritis of the knee: results of the two-year multinational knee osteoarthritis structural arthritis study. Arthritis Rheum 54, 3494-3507.

[11] Birrell, F., Lunt, M., Macfarlane, G., Silman, A., (2005). Association between pain in the hip region and radiographic changes of osteoarthritis: results from a population-based study. Rheumatology (Oxford) 44, 337-341.

[12] Bitton, R., (2009). The economic burden of osteoarthritis. Am.J.Manag.Care 15, S230-S235.

[13] Blagojevic, M., Jinks, C., Jeffery, A., Jordan, K. P., (2010). Risk factors for onset of osteoarthritis of the knee in older adults: a systematic review and meta-analysis. Osteoarthritis.Cartilage. 18, 24-33.

[14] Brandt, K. D., Mazzuca, S. A., (2005). Lessons learned from nine clinical trials of disease-modifying osteoarthritis drugs. Arthritis Rheum 52, 3349-3359.

[15] Brooks, P. M., (2006). The burden of musculoskeletal disease–a global perspective. Clin.Rheumatol. 25, 778-781.

[16] Brouwer, G. M., van Tol, A. W., Bergink, A. P., Belo, J. N., Bernsen, R. M., Reijman, M., Pols, H. A., Bierma-Zeinstra, S. M., (2007). Association between valgus and varus alignment and the development and progression of radiographic osteoarthritis of the knee. Arthritis Rheum 56, 1204-1211.

[17] Buckwalter, J. A., Saltzman, C., Brown, T., (2004). The impact of osteoarthritis: implications for research. Clin.Orthop.Relat Res. S6-15.

[18] Changhai D, Flavia C, Leigh B, et el, (2007). A longitudinal study of sex, age on rate of change in knee cartilage volume in adults. Rheumatology 46, 273-279.

[19] Charnley, J., (1960). The lubrication of animal joints in relation to surgical reconstruction by arthroplasty. Ann Rheum Dis 19, 10-19.

[20] Chiang, E. H., Adler, R. S., Meyer, C. R., Rubin, J. M., Dedrick, D. K., Laing, T. J., (1994). Quantitative assessment of surface roughness using backscattered ultrasound: the effects of finite surface curvature. Ultrasound in medicine & biology 20, 123.

[21] Cicuttini, F., Forbes, A., Morris, K., Darling, S., Bailey, M., Stuckey, S., (1999). Gender differences in knee cartilage volume as measured by magnetic resonance imaging. Osteoarthritis.Cartilage. 7, 265-271.

[22] Connolly, K. D., Ronsky, J. L., Westover, L. M., Kupper, J. C., Frayne, R., (2009). Analysis techniques for congruence of the patellofemoral joint. J.Biomech.Eng 131, 124503.

[23] Coyte, P. C., Asche, C. V., Croxford, R., Chan, B., (1998). The economic cost of musculoskeletal disorders in Canada. Arthritis Care Res. 11, 315-325.

[24] Csintalan, R. P., Schulz, M. M., Woo, J., McMahon, P. J., Lee, T. Q., (2002). Gender differences in patellofemoral joint biomechanics. Clin.Orthop.Relat Res. 260-269.

[25] Dam, E. B., Folkesson, J., Pettersen, P. C., Christiansen, C., (2007). Automatic morphometric cartilage quantification in the medial tibial plateau from MRI for osteoarthritis grading. Osteoarthritis and Cartilage 15, 808-818.

[26] E. B. Dam, M. Loog, C. Christiansen, I. Byrjalsen, J. Folkesson, M. Nielsen, A. A. Qazi, P. C. Pettersen, P. Garnero, and M. A. Karsdal, "Identification of progressors in osteoarthritis by combining biochemical and MRI-based markers," Arthritis Res. Ther., vol. 11, no. 4, p. R115, 2009.

[27] De Gruttola, V. G., Clax, P., DeMets, D. L., Downing, G. J., Ellenberg, S. S., Friedman, L., Gail, M. H., Prentice, R., Wittes, J., Zeger, S. L., (2001). Considerations in the evaluation of surrogate endpoints in clinical trials. summary of a National Institutes of Health workshop. Control Clin.Trials 22, 485-502.

[28] Gupta, S., Hawker, G. A., Laporte, A., Croxford, R., Coyte, P. C., (2005). The economic burden of disabling hip and knee osteoarthritis (OA) from the perspective of individuals living with this condition. Rheumatology (Oxford) 44, 1531-1537.

[29] Dearborn, J. T., Eakin, C. L., Skinner, H. B., (1996). Medial compartment arthrosis of the knee. Am.J.Orthop.(Belle.Mead NJ) 25, 18-26.

[30] DeLong, E. R., DeLong, D. M., Clarke-Pearson, D. L., (1988). Comparing the areas under two or more correlated receiver operating characteristic curves: a nonparametric approach. Biometrics 44, 837-845.

[31] Ding, C., Cicuttini, F., Scott, F., Glisson, M., Jones, G., (2003). Sex differences in knee cartilage volume in adults: role of body and bone size, age and physical activity. Rheumatology (Oxford) 42, 1317-1323.

[32] Drewniak, E. I., Jay, G. D., Fleming, B. C., Crisco, J. J., (2009). Comparison of two methods for calculating the frictional properties of articular cartilage using a simple pendulum and intact mouse knee joints. J.Biomech. 42, 1996-1999.

[33] Dubois, J., Hertz-Pannier, L., haene-Lambertz, G., Cointepas, Y., Le Bihan, D., (2006). Assessment of the early organization and maturation of infants' cerebral white matter fiber bundles: a feasibility study using quantitative diffusion tensor imaging and tractography. Neuroimage 30, 1121-1132.

[34] Dunn, T., Lu, Y., Jin, H., Ries, M., Majumdar, S., (2004). T2 relaxation time of cartilage at mr imaging: comparison with severity of knee osteoarthritis. Radiology 232, 592-598.

[35] Eaton, C. B., (2004). Obesity as a risk factor for osteoarthritis: mechanical versus metabolic. Med.Health R.I. 87, 201-204.

[36] Eckstein, F., Wirth, W., Hudelmaier, M. I., Maschek, S., Hitzl, W., Wyman, B. T., Nevitt, M., Hellio Le Graverand, M. P., Hunter, D., (2009). Relationship of compartment-specific structural knee status at baseline with change in cartilage morphology: a prospective observational study using data from the osteoarthritis initiative. Arthritis Res.Ther. 11, R90.

[37] F M Circuttini, A E Wluka, S L Stuckey, (2001). Tibial and femoral cartilage changes in knee osteoarthritis. Ann Rheum Dis 60, 977-980.

[38] Felson, D. T., Lawrence, R. C., Dieppe, P. A., Hirsch, R., Helmick, C. G., Jordan, J. M., Kington, R. S., Lane, N. E., Nevitt, M. C., Zhang, Y., Sowers, M., McAlindon, T., Spector, T. D., Poole, A. R., Yanovski, S. Z., Ateshian, G., Sharma, L., Buckwalter, J. A., Brandt, K. D., Fries, J. F., (2000). Osteoarthritis: new insights. Part 1: the disease and its risk factors. Ann Intern.Med. 133, 635-646.

[39] Folkesson, J., Dam, E. B., Olsen, O. F., Christiansen, C., (2007). Accuracy evaluation of automatic quantification of the articular cartilage surface curvature from MRI. Acad Radiol 14, 1221-1228.

[40] Folkesson, J., Dam, E. B., Olsen, O. F., Karsdal, M. A., Pettersen, P. C., Christiansen, C., (2008). Automatic quantification of local and global articular cartilage surface curvature: biomarkers for osteoarthritis? Magn Reson.Med 59, 1340-1346.

[41] Folkesson, J., Dam, E. B., Olsen, O. F., Pettersen, P. C., Christiansen, C., (2007). Segmenting Articular Cartilage Automatically Using a Voxel Classification Approach. IEEE Trans.on Medical Imaging 26, 106-115.

[42] Fukubayashi, T., Kurosawa, H., (1980). The contact area and pressure distribution pattern of the knee. A study of normal and osteoarthrotic knee joints. Acta Orthop.Scand. 51, 871-879.

[43] Guermazi, A., Burstein, D., Conaghan, P., Eckstein, F., Hellio Le Graverand-Gastineau MP, Keen, H., Roemer, F. W., (2008). Imaging in osteoarthritis. Rheum Dis Clin.North Am. 34, 645-687.

[44] Hendee, W. R., Morgan, C. J., (1984). Magnetic resonance imaging. Part I–physical principles. West J.Med. 141, 491-500.

[45] Hanna, F. S., Teichtahl, A. J., Wluka, A. E., Wang, Y., Urquhart, D. M., English, D. R., Giles, G. G., Cicuttini, F. M., (2009). Women have increased rates of cartilage loss and progression of cartilage defects at the knee than men: a gender study of adults without clinical knee osteoarthritis. Menopause. 16, 666-670.

[46] Hayashi, N., Watanabe, Y., Masumoto, T., Mori, H., Aoki, S., Ohtomo, K., Okitsu, O., Takahashi, T., (2004). Utilization of low-field MR scanners. Magn Reson.Med.Sci. 3, 27-38.

[47] Hellio Le Graverand-Gastineau, M., (2009). OA clinical trials: current targets and trials for OA. Choosing molecular targets: what have we learned and where we are headed? Osteoarthritis and Cartilage.

[48] Henderson, C. E., Higginson, J. S., Barrance, P. J., (2011). Comparison of MRI-based estimates of articular cartilage contact area in the tibiofemoral joint. J.Biomech.Eng 133, 014502.

[49] Hohe, J., Ateshian, G., Reiser, M., Englmeier, K. H., Eckstein, F., (2002). Surface size, curvature analysis, and assessment of knee joint incongruity with mri in vivo. Magnetic Resonance in Medicine 47, 554-561.

[50] Hunter, D. J., Arden, N., Conaghan, P. G., Eckstein, F., Gold, G., Grainger, A., Guermazi, A., Harvey, W., Jones, G., Hellio Le Graverand, M. P., Laredo, J. D., Lo, G., Losina, E., Mosher, T. J., Roemer, F., Zhang, W., (2011). Definition of osteoarthritis on MRI: results of a Delphi exercise. Osteoarthritis.Cartilage. 19, 963-969.

[51] Hunter, D. J., Guermazi, A., Lo, G. H., Grainger, A. J., Conaghan, P. G., Boudreau, R. M., Roemer, F. W., (2011). Evolution of semi-quantitative whole joint assessment of knee OA: MOAKS (MRI Osteoarthritis Knee Score). Osteoarthritis.Cartilage. 19, 990-1002.

[52] Hunter, D. J., Sharma, L., Skaife, T., (2009). Alignment and osteoarthritis of the knee. J.Bone Joint Surg.Am. 91 Suppl 1, 85-89.

[53] Ihn, J. C., Kim, S. J., Park, I. H., (1993). In vitro study of contact area and pressure distribution in the human knee after partial and total meniscectomy. Int.Orthop. 17, 214-218.

[54] Jackson, B. D., Wluka, A. E., Teichtahl, A. J., Morris, M. E., Cicuttini, F. M., (2004). Reviewing knee osteoarthritis–a biomechanical perspective. J.Sci.Med.Sport 7, 347-357.

[55] Kaleva, E., Saarakkala, S., Jurvelin, J. S., Viren, T., Toyras, J., (2009). Effects of ultrasound beam angle and surface roughness on the quantitative ultrasound parameters of articular cartilage. Ultrasound Med.Biol. 35, 1344-1351.

[56] Kamei, G., Sumen, Y., Sakaridani, K., (2008). Evaluation of cartilage defect at medial femoral condyle in early osteoarthritis of the knee. Magn Reson.Imaging 26, 567-571.

[57] Karsdal, M. A., Leeming, D. J., Dam, E. B., Henriksen, K., Alexandersen, P., Pastoureau, P., Altman, R. D., Christiansen, C., (2008). Should subchondral bone turnover be targeted when treating osteoarthritis? Osteoarthritis Cartilage 16, 638-646.

[58] Kauppila, L. I., Polak, J. F., Cupples, L. A., Hannan, M. T., Kiel, D. P., Wilson, P. W. F., (1997). New indices to classify location, severity

and progression of calcific lesions in the abdominal aorta: a 25-year follow-up study. Atherosclerosis 132, 245-250.

[59] Kaus, M. R., Berg, J., Weese, J., Niessen, W., Pekar, V., (2004). Automated segmentation of the left ventricle in cardiac MRI. Medical Image Analysis 8, 245-254.

[60] Kellgren, J. H., Lawrence, J. S., (1957). Radiological assessment of osteo-arthrosis. Ann Rheum Dis 16, 494-501.

[61] Kirkwood, B. R., Sterne, J. A. C., (2003). Essential medical statistics. Blackwell Publishing.

[62] Kuhnigk, J. M., Hahn, H. K., Hindennach, M., Dicken, V., Krass, S., Peitgen, H. O., (2003). Lung lobe segmentation by anatomy-guided 3D watershed transform.

[63] Lanyon, P., O'Reilly, S., Jones, A., Doherty, M., (1998). Radiographic assessment of symptomatic knee osteoarthritis in the community: definitions and normal joint space. Ann Rheum Dis 57, 595-601.

[64] Lawrence, R. C., Felson, D. T., Helmick, C. G., Arnold, L. M., Choi, H., Deyo, R. A., Gabriel, S., Hirsch, R., Hochberg, M. C., Hunder, G. G., Jordan, J. M., Katz, J. N., Kremers, H. M., Wolfe, F., (2008). Estimates of the prevalence of arthritis and other rheumatic conditions in the United States. Part II. Arthritis Rheum 58, 26-35.

[65] Lawrence, R. C., Helmick, C. G., Arnett, F. C., Deyo, R. A., Felson, D. T., Giannini, E. H., Heyse, S. P., Hirsch, R., Hochberg, M. C., Hunder, G. G., Liang, M. H., Pillemer, S. R., Steen, V. D., Wolfe, F., (1998). Estimates of the prevalence of arthritis and selected musculoskeletal disorders in the United States. Arthritis Rheum 41, 778-799.

[66] Ledingham, J., Regan, M., Jones, A., Doherty, M., (1993). Radiographic patterns and associations of osteoarthritis of the knee in patients referred to hospital. Ann Rheum Dis 52, 520-526.

[67] Lee, S. J., Aadalen, K. J., Malaviya, P., Lorenz, E. P., Hayden, J. K., Farr, J., Kang, R. W., Cole, B. J., (2006). Tibiofemoral contact mechanics

after serial medial meniscectomies in the human cadaveric knee. Am.J.Sports Med. 34, 1334-1344.

[68] Li, G., Park, S. E., DeFrate, L. E., Schutzer, M. E., Ji, L., Gill, T. J., Rubash, H. E., (2005). The cartilage thickness distribution in the tibiofemoral joint and its correlation with cartilage-to-cartilage contact. Clin.Biomech.(Bristol., Avon.) 20, 736-744.

[69] Link, T. M., Steinbach, L. S., Ghosh, S., Ries, M., Lu, Y., Lane, N., Majumdar, S., (2003). Osteoarthritis: MR imaging findings in different stages of disease and correlation with clinical findings. Radiology 226, 373-381.

[70] Lo, G. H., Hunter, D. J., Nevitt, M., Lynch, J., McAlindon, T. E., (2009). Strong association of MRI meniscal derangement and bone marrow lesions in knee osteoarthritis: data from the osteoarthritis initiative. Osteoarthritis. Cartilage. 17, 743-747.

[71] Maleki-Fischbach, M., Jordan, J. M., (2010). New developments in osteoarthritis. Sex differences in magnetic resonance imaging-based biomarkers and in those of joint metabolism. Arthritis Res.Ther. 12, 212.

[72] McKean, K. A., Landry, S. C., Hubley-Kozey, C. L., Dunbar, M. J., Stanish, W. D., Deluzio, K. J., (2007). Gender differences exist in osteoarthritic gait. Clin.Biomech. (Bristol., Avon.) 22, 400-409.

[73] Naka, M. H., Hattori, K., Ikeuchi, K., (2006). Evaluation of the superficial characteristics of articular cartilage using evanescent waves in the friction tests with intermittent sliding and loading. J.Biomech. 39, 2164-2170.

[74] Neu, C. P., Reddi, A. H., Komvopoulos, K., Schmid, T. M., Di Cesare, P. E., (2010). Increased friction coefficient and superficial zone protein expression in patients with advanced osteoarthritis. Arthritis Rheum 62, 2680-2687.

[75] O'Connor, M. I., (2006). Osteoarthritis of the hip and knee: sex and gender differences. Orthop.Clin.North Am. 37, 559-568.

[76] O. Beuf, S. Ghosh, D. C. Newitt, T. M. Link, L. Steinbach, M. Ries, N. Lane, and S. Majumdar, "Magnetic resonance imaging of normal and osteoarthritic trabecular bone structure in the human knee," Arthritis Rheum, vol. 46, no. 2, pp. 385-393, Feb.2002.

[77] Otterness, I. G., Eckstein, F., (2007). Women have thinner cartilage and smaller joint surfaces than men after adjustment for body height and weight. Osteoarthritis. Cartilage. 15, 666-672.

[78] Peterfy, C. G., Guermazi, A., Zaim, S., Tirman, P. F., Miaux, Y., White, D., Kothari, M., Lu, Y., Fye, K., Zhao, S., Genant, H. K., (2004). Whole-Organ Magnetic Resonance Imaging Score (WORMS) of the knee in osteoarthritis. Osteoarthritis. Cartilage. 12, 177-190.

[79] Peterfy, C. G., Gold, G., Eckstein, F., Cicuttini, F., Dardzinski, B., Stevens, R., (2006). MRI protocols for whole-organ assessment of the knee in osteoarthritis. Osteoarthritis.Cartilage. 14 Suppl A, A95-111.

[80] Patel, V. V., Hall, K., Ries, M., Lotz, J., Ozhinsky, E., Lindsey, C., Lu, Y., Majumdar, S., (2004). A three-dimensional MRI analysis of knee kinematics. J.Orthop.Res. 22, 283-292.

[81] Pritzker, K. P., Gay, S., Jimenez, S. A., Ostergaard, K., Pelletier, J. P., Revell, P. A., Salter, D., van den Berg, W. B., (2006). Osteoarthritis cartilage histopathology: grading and staging. Osteoarthritis Cartilage 14, 13-29.

[82] Qvist, P., Bay-Jensen, A. C., Christiansen, C., Dam, E. B., Pastoureau, P., Karsdal, M. A., (2008). The disease modifying osteoarthritis drug (DMOAD): Is it in the horizon? Pharmacol.Res. 58, 1-7.

[83] Raundahl, J., Loog, M., Pettersen, P., Tanko, L. B., Nielsen, M., (2008). Automated effect-specific mammographic pattern measures. IEEE Trans.Med Imaging 27, 1054-1060.

[84] Reginster, J. Y., (2002). The prevalence and burden of arthritis. Rheumatology (Oxford) 41 Supp 1, 3-6.

[85] Segal, N. A., Anderson, D. D., Iyer, K. S., Baker, J., Torner, J. C., Lynch, J. A., Felson, D. T., Lewis, C. E., Brown, T. D., (2009). Baseline articular contact stress levels predict incident symptomatic knee osteoarthritis development in the MOST cohort. J.Orthop.Res. 27, 1562-1568.

[86] J. A. Sethian, (1996). A fast marching level set method for monotonically advancing fronts. Proc. Natl. Acad. Sci. U. S. A, vol. 93, no. 4, pp. 1591-1595.

[87] Shan-hua Qian, Shi-rong Ge, Qing-liang Wang, (2011). The Frictional Coefficient of Bovine Knee Articular Cartilage. pp. 79-85.

[88] Sondergaard, B. C., Henriksen, K., Wulf, H., Oestergaard, S., Schurigt, U., Brauer, R., Danielsen, I., Christiansen, C., Qvist, P., Karsdal, M. A., (2006). Relative contribution of matrix metalloprotease and cysteine protease activities to cytokine-stimulated articular cartilage degradation. Osteoarthritis Cartilage 14, 738-748.

[89] Spector, T. D., Conaghan, P. G., Buckland-Wright, J. C., Garnero, P., Cline, G. A., Beary, J. F., Valent, D. J., Meyer, J. M., (2005). Effect of risedronate on joint structure and symptoms of knee osteoarthritis: results of the BRISK randomized, controlled trial [ISRCTN01928173]. Arthritis Research and Therapy 7, R625-R633.

[90] Srikanth, V. K., Fryer, J. L., Zhai, G., Winzenberg, T. M., Hosmer, D., Jones, G., (2005). A meta-analysis of sex differences prevalence, incidence and severity of osteoarthritis. Osteoarthritis.Cartilage. 13, 769-781.

[91] T. L. Donahue, M. L. Hull, M. M. Rashid, and C. R. Jacobs, (2002). A finite element model of the human knee joint for the study of tibio-femoral contact, J. Biomech. Eng, vol. 124, no. 3, pp. 273-280.

[92] Sudhakar Tummala, Erik B Dam, (2010). Surface smoothness: cartilage biomarkers for knee OA beyond the radiologist.

[93] Teeple, E., Elsaid, K. A., Fleming, B. C., Jay, G. D., Aslani, K., Crisco, J. J., Mechrefe, A. P., (2008). Coefficients of friction, lubricin, and

cartilage damage in the anterior cruciate ligament-deficient guinea pig knee. J.Orthop.Res. 26, 231-237.

[94] Teeple, E., Fleming, B. C., Mechrefe, A. P., Crisco, J. J., Brady, M. F., Jay, G. D., (2007). Frictional properties of Hartley guinea pig knees with and without proteolytic disruption of the articular surfaces. Osteoarthritis.Cartilage. 15, 309-315.

[95] Taekema, D. G., Ling, C. H., Blauw, G. J., Meskers, C. G., Westendorp, R. G., de Craen, A. J. et al. Circulating levels of IGF1 are associated with muscle strength in middle-aged- and oldest-old women. Eur.J.Endocrinol. 2011; 164(2):189-196.

[96] Terukina, M., Fujioka, H., Yoshiya, S., Kurosaka, M., Makino, T., Matsui, N., Tanaka, J., (2003). Analysis of the thickness and curvature of articular cartilage of the femoral condyle. Arthroscopy 19.

[97] Valdes, A. M., Loughlin, J., Timms, K. M., van Meurs, J. J., Southam, L., Wilson, S. G., Doherty, S., Lories, R. J., Luyten, F. P., Gutin, A., Abkevich, V., Ge, D., Hofman, A., Uitterlinden, A. G., Hart, D. J., Zhang, F., Zhai, G., Egli, R. J., Doherty, M., Lanchbury, J., Spector, T. D., (2008). Genome-wide association scan identifies a prostaglandin-endoperoxide synthase 2 variant involved in risk of knee osteoarthritis. Am.J.Hum.Genet. 82, 1231-1240.

[98] Van Leemput, K., Maes, F., Vandermeulen, D., Suetens, P., (1999). Automated model-based tissue classification of MR images of the brain. IEEE Transactions on Medical Imaging 18, 897-908.

[99] Walker, P. S., Erkman, M. J., (1975). The role of the menisci in force transmission across the knee. Clin.Orthop.Relat Res. 184-192.

[100] Warfield, S. K., Zou, K. H., Wells, W. M., (2004). Simultaneous Truth and Performance Level Estimation (STABLE): An algorithm for the validation of Image Segmentation. IEEE Transactions on Medical Imaging 23, 903-921.

[101] Westin, C. F., Maier, S. E., Mamata, H., Nabavi, A., Jolesz, F. A., Kikinis, R., (2002). Processing and visualization for diffusion tensor MRI. Medical Image Analysis 6, 93-108.

List of Publications

Peer-reviewed journal papers

• Tummala S, Bay-Jensen AC, Karsdal M, Dam EB, "Diagnosis of Osteoarthritis by Cartilage Surface Smoothness Quantified Automatically from Knee MRI." *Cartilage*, vol 2 (1), 50-59, 2011
• Tummala S, Nielsen M, Christiansen C, Dam EB, "Automatic Quantification of Tibio-Femoral Contact Area and Congruity." *IEEE Transactions on Medical Imaging* (under re-revision)
• Tummala S, Schiphof D, Byrjalsen I, Dam EB, "Gender differences in Tibio-Femoral Contact Area and Congruity from MRI." *Osteoarthritis & Cartilage* (under review)

Peer-reviewed conference papers

• Tummala S, Dam EB, "Surface Smoothness: Cartilage biomarkers for knee OA beyond the radiologist." *SPIE Medical Imaging*, San Diego, 2010
• Tummala S, Dam EB, Nielsen M, "Automatic Quantification of Congruity from Knee MRI." *MICCAI Computational Biomechanics for Medicine Workshop 6*, Toronto, 2011

Peer-reviewed conference abstracts

• Tummala S, Karsdal M, Bay-Jensen AC, Dam EB, "Tibial and Femoral Cartilage Smoothness: Diagnostic Markers of Early Osteoarthritis." *OARSI*,

Montreal, 2009

• Tummala S, Pettersen P, Dam EB, "Tibio-femoral Contact Area Quantification for Investigation of Early Osteoarthritis." *OARSI*, Brussels, 2010.

• Tummala S, Dam EB, Nielsen M, "Diagnosis of Early OA by Automatic Quantification of Congruity from Knee MRI." *OARSI*, San Diego, 2011 (Oral)

Acknowlegements

First and foremost, I would like to thank my supervisor Erik B Dam for excellent supervision and support during the project, and from whom I have learned a lot! I would also like to thank my co-supervisor Mads Nielsen for occasional peptalks and for sharing his view on the larger context in which the project fits.
I also owe thanks to all the people at BiomedIQ A/S, both current and former members, who all contributed to a pleasant and great working environment. Special thanks go to the people at Nordic Bioscience A/S with whom I colloborated during the first half of my PhD.
Finally, thanks to my parents Basaveswara Rao and Ratna Kumari and my younger brother Prasanth for always supporting me from India during my PhD.